C.J. Meerman

Asymptotic analysis on blow-up solutions of the Generalized Korteweg-de Vries equation

Master thesis, August 2012

Supervisor: Dr. V. Rottschäfer

Mathematisch Instituut, Universiteit Leiden

Contents

1 Introduction

In this thesis we analyse the Generalized Korteweg-de Vries (GKdV) equation of the following form

$$\frac{\partial \phi}{\partial t} + \frac{\partial}{\partial x}\left(\frac{\partial^2 \phi}{\partial x^2} + \phi^p\right) = 0, \tag{1.1}$$

with initial condition

$$\phi(x, 0) = \phi_0(x),$$

where $\phi(x, t) \in \mathbb{R}$ and $p \in \mathbb{R}$ a parameter.

We are particularly interested in solutions of equation (1.1) which show blow-up behaviour. Blow-up for the GKdV equation occurs at some blowup time $T < \infty$ where

$$\max_x |\phi(x, t)| \to \infty \text{ as } t \uparrow T,$$

with $|\phi(x, t)| < \infty$ for all $t < T, x \in \mathbb{R}$.

Equation (1.1) is derived from the original Korteweg-de Vries equation, which we obtain by setting $p = 2$. This nonlinear partial differential equation arises in many physical systems, e.q. water waves, plasma physics, anharmonic lattices and elastic rods,[11], [7]. The case $p = 3$, which is known as the Modified Korteweg-de Vries equation, can be transformed into the original Kortweg-de Vries equation by the Miura transformation, [1].

The GKdV equation first appeared in the study of waves on shallow water,[6]. Together with the nonlinear Schrödinger equation, these equations can be considered as universal models for Hamiltonian systems in infinite dimensions. Since equation (1.1) is Hamiltonian, there is conservation of energy, meaning that the amount of energy is constant through time.

$$E(\phi(t)) = \frac{1}{2}\int_{\mathbb{R}} \phi_x(x, 0)^2 \; - \frac{1}{p-1}\phi(x, 0)^{p+1} \; dx.$$

Conservation of mass is also upheld, where the mass is given by

$$M(\phi(t)) = \int_{\mathbb{R}} \phi(x, 0)^2 \; dx. \tag{1.2}$$

Therefore, the L^2-norm does not blow up.

Using the Gagliardo-Nirenberg inequality,[16], an a priori bound can be estimated

$$||\phi(t)||_{H^1_x(\mathbb{R})} \leq C(M(\phi_0), H(\phi_0)),$$

for some quantity $C(M(\Phi_0), H(\Phi_0))$, depending on the initial mass and energy.

Note that this estimation implies that all solutions are bounded for $p < 5$, regardless the amount of mass. For $p = 5$, the Gagliardo-Nirenberg inequality is only valid for sufficiently small mass. For $p > 5$, the a priori estimate fails to provide this conclusion. The borderline case $p = 5$ has already been studied thoroughly where solutions in the energy space $H^1(\mathbb{R})$ are analysed. Assuming the energy of the initial condition to be

nonpositive and a restriction on the initial condition, the existence of blow-up solutions in finite or infinite time in H^1 is proved in [10]. In [8] the authors prove that the solutions blow up in finite time if the initial data has a certain decay. Moreover, an upper bound on the blow-up rate is given. In [9], the profile of the solution around the bump at blow-up time is being studied. First a rescaling and translation are introduced. Then, the authors prove that solutions converge to a universal profile locally in space at the blow-up time T, provided that the initial mass is close to the minimal mass allowing blow-up.

The case $p = 5$ is not only the borderline case for blow-up solutions, but also for the stability of the solutions. For all $p \geq 2$, explicit solitary (travelling) wave solutions of the GKdV equation are known, see [5],

$$\Phi(x,t;C,x_0) = \left\{ \frac{p+1}{2} C \operatorname{sech}^2 \left(\frac{p-1}{2} \sqrt{C}(x - x_0 - Ct) \right) \right\}^{\frac{1}{p-1}}, \tag{1.3}$$

where $C > 0$ is the wave speed and x_0 the translation parameter. Blow-up occurs in the case when a solitary wave becomes unstable whereafter its maximum starts to grow and the solution becomes unbounded (in finite time). For $p = 2, 3, 4$, this family of solutions is known to be (asymptotically) stable to perturbations. This means that if the initial condition is chosen to be $\phi_0 = \Phi(x, 0; C, x_0) + u(x)$, with $u(x)$ a small perturbation, the solution $\phi(x,t)$ tends toward $\Phi(x,t;\tilde{C},\tilde{x_0})$ for some other parameters $\tilde{C}$ and $\tilde{x_0}$ as $t \to \infty$, [12]. For $p \geq 5$, even weaker statements of stability, such are orbital stability, are known to be false, [3].

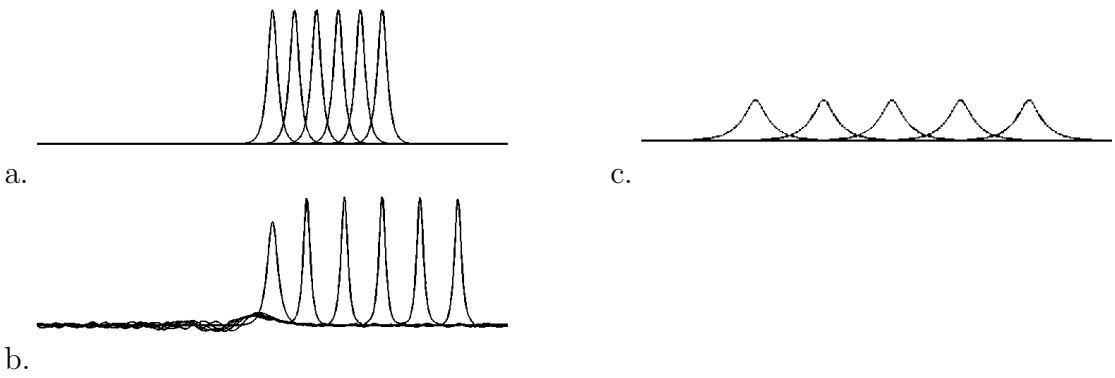

Figure 1: Solutions as found in the preliminary numerical simulations performed by J.F. Williams for the GKdV for $p = 4$ (a, b) and for $p = 6$ (c) starting with different initial conditions. The initial condition and solutions at several equidistant time-steps are given. Figures (a – c) show solitary waves where the soliton in (b) has a dispersive tail.

The GKdV equation is also dispersive. Therefore, different components of the solution $\phi(x,t)$ travel at different velocities, each of them determined by their frequency. Consequently, it often happens that the components are so dispersed, that the solution appears to have a much smaller amplitude at later time, see figure 1. For $p = 2, 3$, this phenomenon is analytically understood using the method of inverse scattering transform, [15], [4]. For $p \geq 4$, the evidence of this phenomenon are limited to observations of numerical simulations. For $p \geq 5$, any solitary wave becomes unstable. If the solution blows up, it will cease to look like a solitary wave. In [5], the authors aim to find out the exact structure of these solutions. It turns out that even slightly perturbed solitary wave profiles as initial condition lead to solutions of the GKdV equation that blow up in finite time.

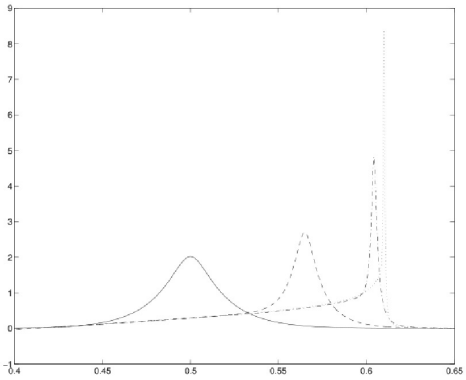

Figure 2: A solution at four different times for $p = 5$ found in the numerical simulations performed by D.B. Dix and W.R. McKinney, see [5]. The initial profile is centered at $x = 0.5$; the bump moves to the right and grows in height as t increases.

As shown in figure 2, the initial solution has a bump around $x = 0.5$. As time increases, the solution moves to the right and the height of the bump grows, the width narrows in the process and the bump appears to blow up in finite time. It seems that the solution possesses a self-similar structure, however, note that the solution does not stay symmetric. The decay on the right-hand side of the bump is faster compared to the left-hand side. Similar results are shown in chapter 2, where numerical simulations for various values of p and different initial conditions are performed. The speed of the solution does not only depend on the intial condition, but also on the time-variable. In some cases, a second bump occurs to the right-hand side of the larger bump.

In the other chapters, we perform an asymptotic analysis to construct the solutions of equation (1.1) which show blow-up in finite time. To scale out the blow-up, a so-called dynamical rescaling is performed in chapter 3. Since the solution is travelling, we also introduce a new variable, $\xi = L(t)^{-\beta}\left(x + cL(t)^{\beta-\gamma}\right)$, with β, γ positive constants. Note that this variable is changing in time. This rescaling reduces equation (1.1) to the third-order partial differential equation

$$v_{\xi\xi\xi} + (|v|^{p-1}v)_\xi - c(\beta-\gamma)v_\xi + L^\gamma\beta\left[\frac{2}{p-1}v + \xi v_\xi\right] + L^{3\beta}v_t = 0, \tag{1.4}$$

where $v(\xi,t) = L(t)^{\alpha}\phi(x,t)$ and $L(t) \to 0$ as $t \uparrow T$. The function $v(\xi,t)$ is assumed to be bounded, which implies that the function $\phi(\xi,t)$ indeed blows up.

We analyse equation (1.4) in various region of the ξ-axis by using asymptotic analysis. We define a so-called bump region, where the maximum of the solution occurs, and the far field for ξ large, see figure 3. First we examine the solution in a region around $\xi = 0$, in the bump region defined by $|\xi| \ll L^{-\gamma}$. In the analysis, we assume that the maximum of the solution lies at $\xi = 0$. After substitution of a regular asymptotic expansion, $v(\xi) = v_0(\xi) + L^{\gamma}v_1(\xi) + \text{h.o.t.}$, the leading order equation is studied. The solution is exponentially decaying. Also an expression for one higher order term of the expansion, v_1, is constructed, which is exponentially increasing. The far field is defined for $|\xi| \gg 1$. We analyse the equation for $|\xi| \gg 1$ and an explicit algebraically decaying solution is obtained using separation of variables.

The solutions of the bump region have exponential behaviour and the solutions of the far field are algebraically, therefore, the two regions cannot be matched together directly, thus, an intermediate region is introduced. The resulting equation has a turning point at $\xi_{tp} = \frac{d}{\beta}L^{-\gamma}$. At this point the behaviour of the solution changes from elliptic to parabolic. For all values of p, solutions to this equation are known.

For general p, the solution in the bump region is matched with the solutions in the far field, see chapter 4. To the left-hand side of the bump region, the solutions in the bump region and the far field are matched to each other by using the elliptic structure of the solutions in the intermediate region. To the right-hand side of the bump region, the solution in the bump region is matched to the elliptic solution whereas the solution in the far field is matched to the parabolic solution in the intermediate region at the left-hand side of the bump region. Matching solutions for equation (1.1) is also done in [5], where the authors match the self-similar part of the solution numerically to the solution more removed from the blow-up part.

Since v_1 is exponentially growing and v_0 is exponentially decaying, this is a priori not the case. Therefore, we need to assume certain restrictions, namely that $L^{\gamma}|v_1| \ll |v_0|$ in the bump region. This method is based on the approach taken for the Ginzburg-Landau equation in [14]. There are two approaches to achieve this condition; the first one is by choosing the constant A_2 in a convenient way and the second approach is to redefine the bump region. These two approaches will be done in chapters 4.

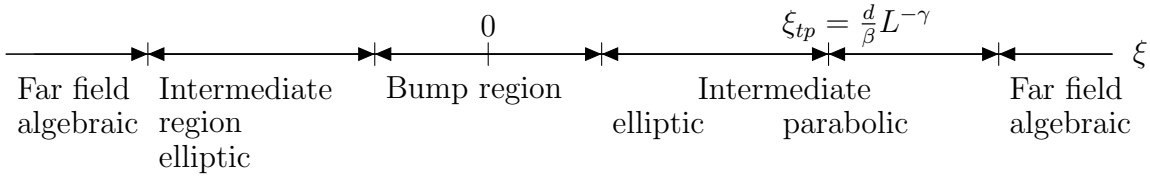

Figure 3: The different points and intervals on the ξ-axis. In the region around $\xi = 0$, the bump solution is found. For $|\xi| \gg 1$ we analyse the far field equation. To match the solutions in these two regions we introduce an intermediate region. At the turning point $\xi_{tp} > 0$, the behaviour of the solutions changes from elliptic to parabolic.

2 Numerical Simulations

In this chapter, numerical simulations of the solutions to equation (1.1) are performed for various values of p and different initial conditions. The simulations are done by using a Matlab code developed by Paul Zegeling (Utrecht University). Hereby we want to thank Paul for letting us use his code.

We are interested in the behaviour when solution (1.3) is slightly perturbed. Therefore, as an initial condition we take

$$\Phi(x,0;0.03,0) = \tilde{C}\left[\left(\frac{0.03(p+1)}{2.0}\right)\operatorname{sech}^2\left(\frac{p-1}{2}\sqrt{0.03}x\right)\right]^{\frac{1}{p-1}},$$

with $\tilde{C}$ a perturbation, which is varied in the different simulations. The initial solution, which has a bump occuring at $x = 0$, is iterated forward in time. The step size of the iterations is equal in all simulations. However, when varying the constant $\tilde{C}$, the step size of the plots is varied as well, to make the plots more readible.

The results of several simulations are shown below, where the initial condition is given in black, the solutions for $p = 5$ in magenta, for $p = 6$ in red, for $p = 7$ in blue and for $p = 8$ in green. First, the results are shown for $\tilde{C} = 0.98$ and the various p-values. Then the simulations for $p = 6, 7, 8$, are shown. The results for $\tilde{C} = 1.00$ are given in figure 6 and for $\tilde{C} = 1.02$ in figure 7, where the simulations for $p = 5$ and $\tilde{C} = 1.00, 1.02$ are given in figure 9. These results are shown separately since the structure of the solutions is not similar to the simulations of the other p-values using the same initial condition. As can be seen in the various figures, the simulations behave similar when fixing the constant $\tilde{C}$ and varying p from $p = 6$ to $p = 8$.

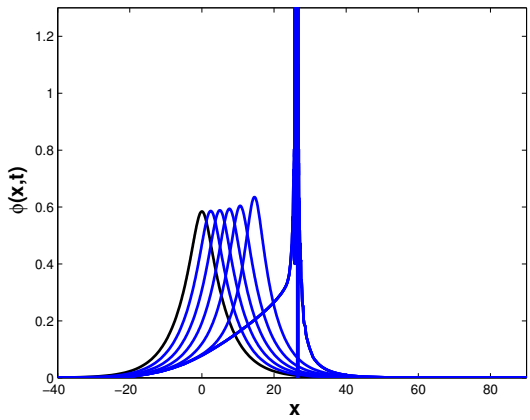

Figure 4: Simulation with $p = 8$ and $\tilde{C} = 1.00$ until the solution blows up. The last solution, when blow-up actually occurs, causes the vertical stripes.

In figure 4, the solution is shown up to and including when the blow-up has occured. The last solution causes the vertical stripes, therefore, the other plots are obscured. To make the simulations in figures 6 and 7 more clear, we do not give the plot of the solution

once blow-up has occured, i.e. the last time-step of figure 4. This blow-up only occurs when we choose $\tilde{C} = 1.00$ and $\tilde{C} = 1.02$. Since there seems to be no blow-up when $\tilde{C} = 0.98$, those simulations were stopped after a random amount of iterations. Thus, we indeed find that blow-up behaviour depends on the initial condition.

For $\tilde{C} = 0.98$, it is not exactly clear what the behaviour of the solutions is, although it is quite similar for the different p-values. All the simulations show a solution with a structure, which clearly travels, to the right for $p = 5$,5a, and $p = 6$, 5b, and to the left for $p = 7$, 5c, and $p = 8$, 5d. In time, the solution starts to show some oscillating behaviour on the left-hand side of the bump. The intensity of this behaviour depends on the p-value, namely, for a higher value of p, the solution starts to oscillate more.

As mentioned before, we give in figures 6 and 7 the solutions up to but not including the last one. In the last solution the actual blow-up occurs, as in figure 4, however, we choose to not give that solution, since it makes the other time-frames less visible.

Although all plots are equidistant, the time between the simulations in figure 6 is larger than the time between the plots in figure 7. Comparing the figures 6 and 7, we conclude that the initial condition as well as the value of p influence the blow-up time. For a higher value of p, or for a higher value of $\tilde{C}$, respectively, the solution blows up faster, hence, the blow-up time is smaller.

We also note that the structure of the solution is quite similar for the various simulations. As time increases, the initial solution, with a bump at $x = 0$, starts to move to the right. Simultaneously, the width of the bump becomes narrower and the height increases. Moreover, the solution loses the symmetric structure. We see that on the right-hand side of the bump, the solutions decay much faster to zero than on the left-hand side of the bump. For a lower value of p, or a higher value of $\tilde{C}$, this phenomenon becomes more visible. Moreover, in figure 7, it seems that a second bump occurs at the left-hand side of the big bump. The described structure is clearly visible in figure 8, where the first and last solutions are plotted for $p = 6$ with $\tilde{C} = 1.00$, 8a, and $\tilde{C} = 1.02$, 8b, and for $p = 5$, with $C = \tilde{1}.00$, 8c, and $\tilde{C} = 1.02$, 8c.

At last we note that the distance between the x-variable of the maxima of two consecutive solutions becomes larger as times proceeds. Therefore, the speed of the solution is increasing as time increases.

In figure 9, simulations are shown for $p = 5$ with $\tilde{C} = 1.00$, 9a, and 9c, and $\tilde{C} = 1.02$, 9b, and 9d, for different lengths of the x-axis. In figures 9c and 9d, the x-interval is longer, though in all simulations, the solution seems to blow up near the boundary of the domain. This is a numerically problem, though it is already known that the borderline case $p = 5$ is numerically very hard to solve, see [5]. However, it is possible that the solution does not blow up because $\tilde{C}$ is chosen too small. Therefore, it would be interesting to study the case $p = 5$ numerically with larger values of $\tilde{C}$.

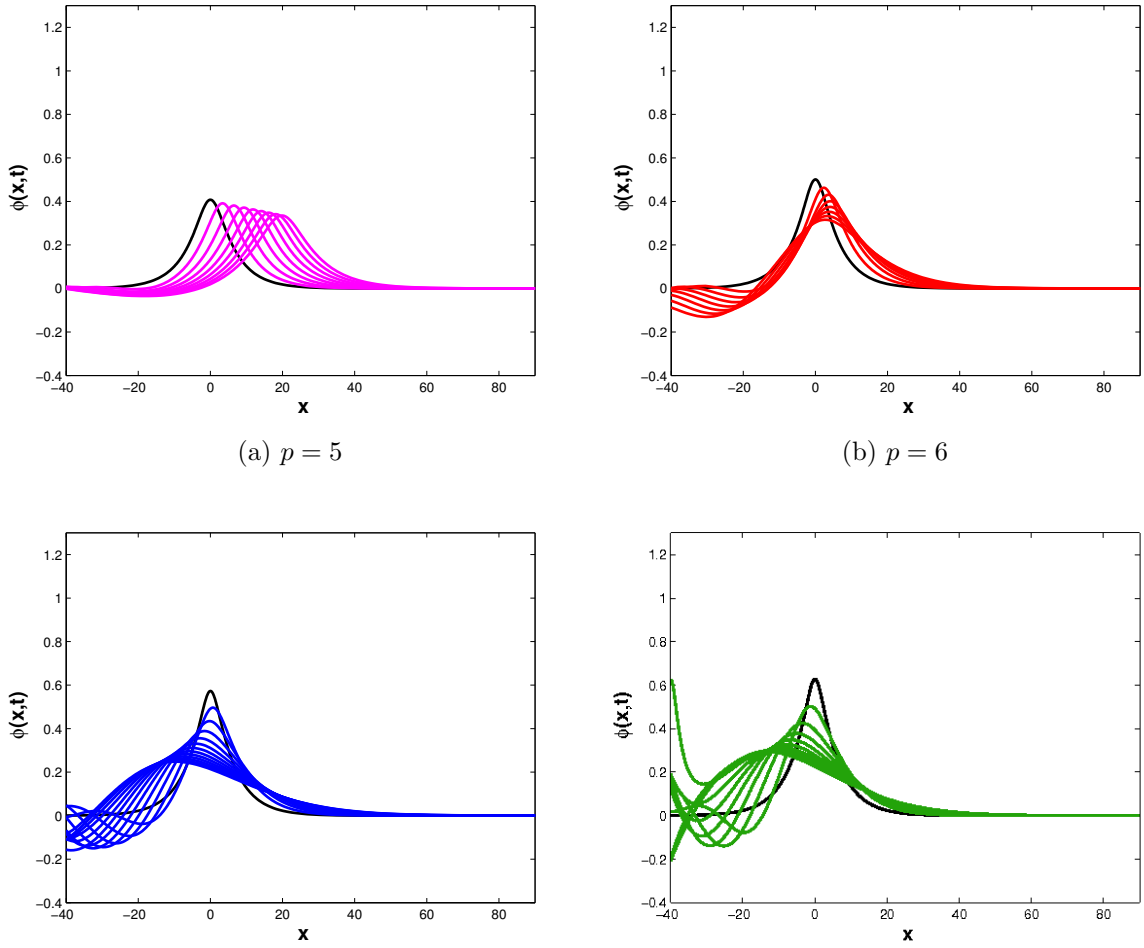

(a) $p = 5$

(b) $p = 6$

(c) $p = 7$

(d) $p = 8$

Figure 5: Simulations for $p = 5, 6, 7, 8$ and $\tilde{C} = 0.98$, where the initial condition is given in black. All solutions appear to have a travelling structure, to the right for $p = 5, 6$, and to the left for $p = 6, 7$. For $p = 5$, see figure (a), the solution seems to maintain its shape, while it decreases in time. For the other values of p, see figures (b) - (d), the solutions appear to start oscillating on the left-hand side of the big bump. Therefore, it is plausible to assume that the solutions obtain a completely different structure than the initial condition. For a higher value of p, the oscillating behaviour of the solution is more intense.

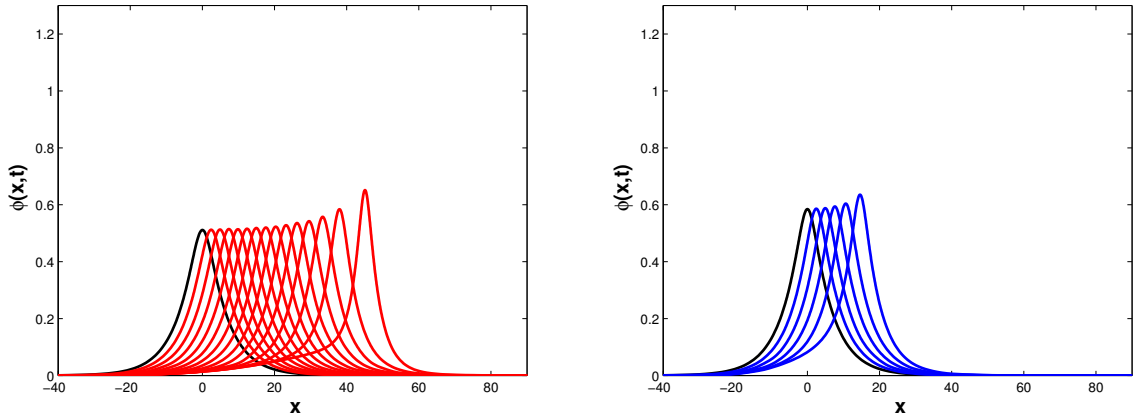

(a) $p = 6$

(b) $p = 7$

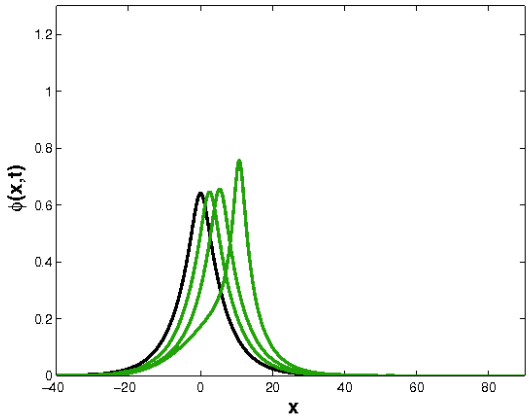

(c) $p = 8$

Figure 6: Simulations for $p = 6, 7, 8$ and $\tilde{C} = 1.00$, where the initial condition is shown in black. The different plots are equidistant and the simulations are stopped one iteration before blow-up would occur. The solution shows a travelling behaviour to the right. The bump of the initial condition becomes narrower in time, while simultaneously, the height of the bump grows. The solution loses the symmetric structure, showing faster decay on the right-hand side of the bump, compared to the left-hand side. The simulations are stoppend one iteration before the blow-up would occur. We can conclude for a higher value of p, the solution becomes less symmetric. The time between the different plots is similar for all values of p, therefore, the blow-up time depends on the value of p. For a higher value of p, the solution blows up faster, hence, the blow-up time becomes smaller. Also, the speed of the solution is increasing, since the distance between the x-variable of the maxima of two consecutive solutions becomes larger in time.

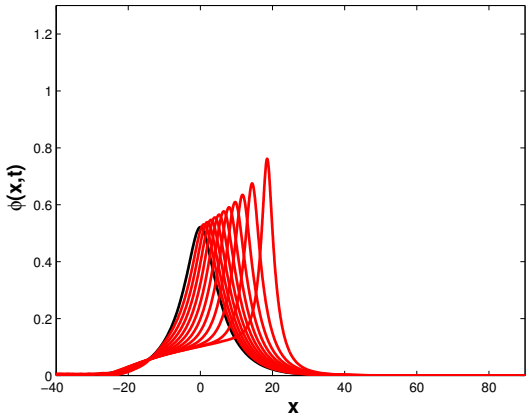

(a) $p = 6$

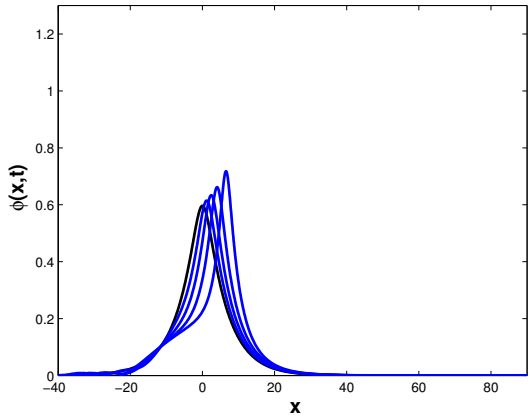

(b) $p = 7$

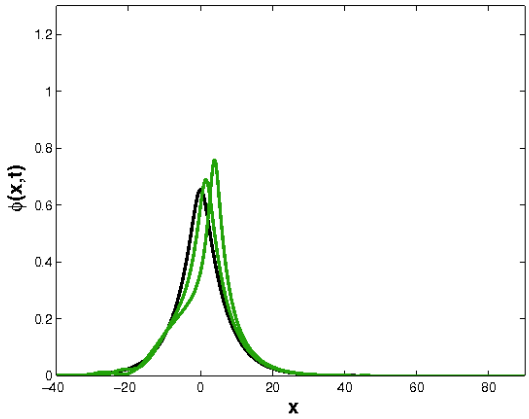

(c) $p = 8$

Figure 7: Simulations for $p = 6, 7, 8$ and $\tilde{C} = 1.02$, with the initial condition shown in black. Again, the simulations are stoppend one iteration before the blow-up would occur. The different plots are equidistant, but the time between the plots is bigger compared to the simulation in figure 6. Hence, we conclude that the blow-up time also depends on the initial condition. For a higher value of $\tilde{C}$, the solution blows up faster, hence, the blow-up time is smaller. The solutions show similar behaviour compared to the simulation in figure 6, although the solutions seem to be even less symmetric. Therefore, for a higher value of $\tilde{C}$, the solution becomes less symmetric. Moreover, it seems that a second bump appears at the left-hand side of the big bump.

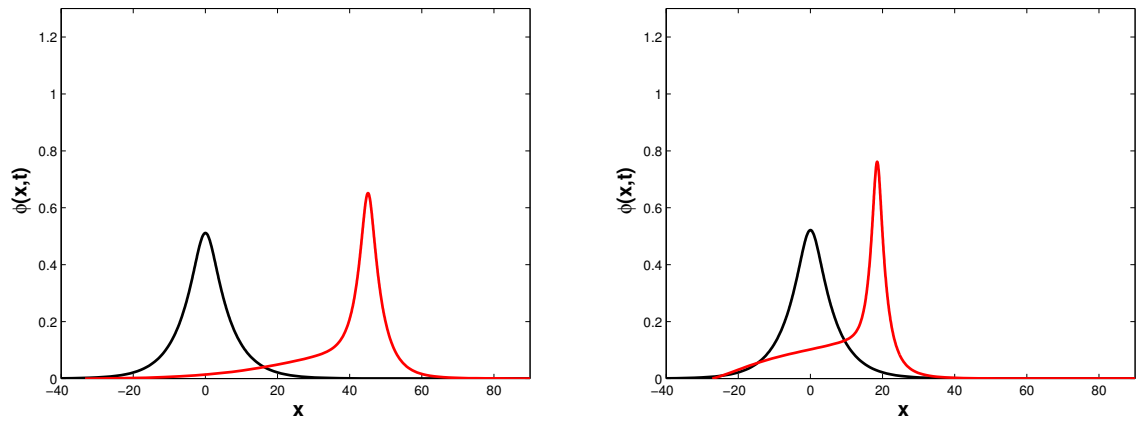

(a) $p = 6, \tilde{C} = 1.00$

(b) $p = 6, \tilde{C} = 1.02$

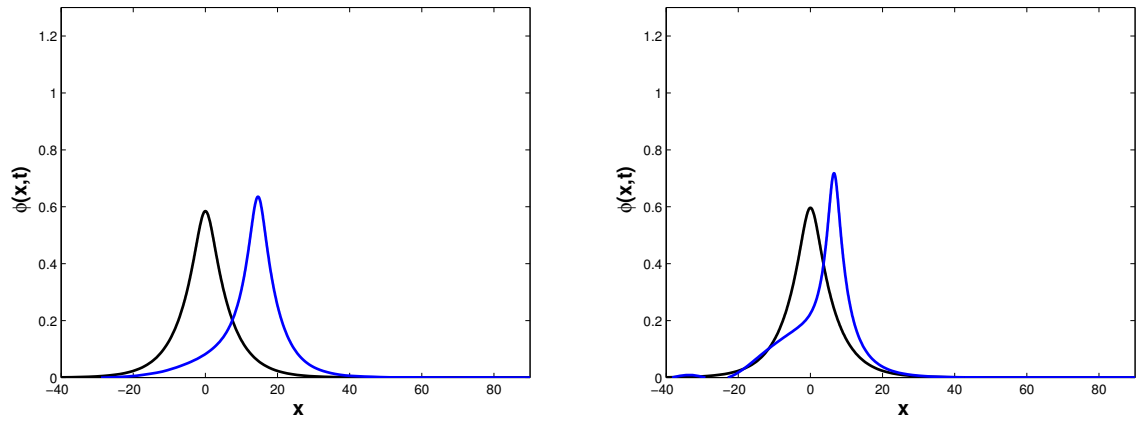

(c) $p = 7, \tilde{C} = 1.00$

(d) $p = 7, \tilde{C} = 1.02$

Figure 8: Simulations for $p = 6, 7$ with $\tilde{C} = 1.00, 1.02$. Only the initial solution, in black, and the solution before blow-up would actually occur, are given. Note that the colored solutions do no longer have a symmetric structure, and we conclude that for a higher value of $\tilde{C}$, the solution becomes less symmetric. Clearly, for a higher value of p, or for a higher value of $\tilde{C}$, respectively, the solution blows up faster, hence, the blow-up time is smaller. The solutions also show a faster decay on the right-hand side of the bump compard to the left-hand side. For $\tilde{C} = 1.02$ and $p = 6$, (b), and $p = 7$, (d), a second bump seems to start appearing on the left-hand side of the bump.

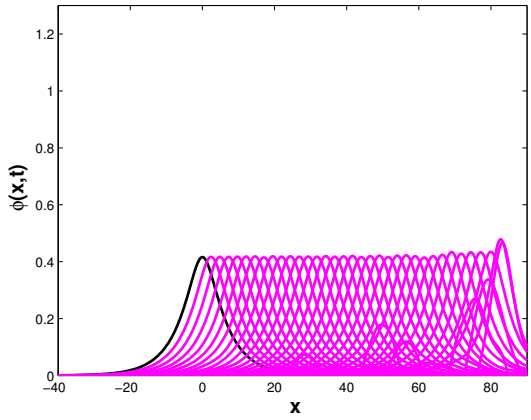

(a) $IC = 1.00$

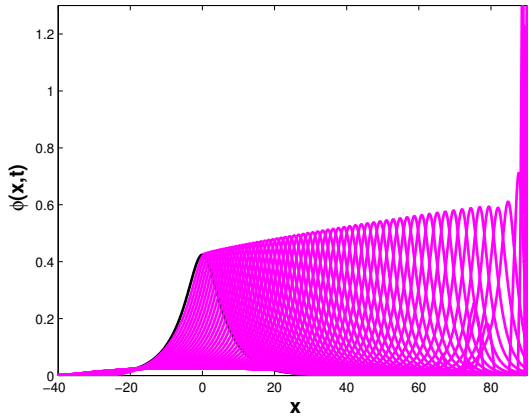

(b) $IC = 1.02$

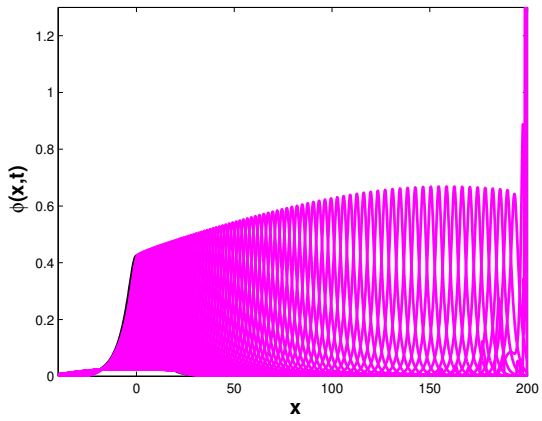

(c) $IC = 1.00$, longer x-axis

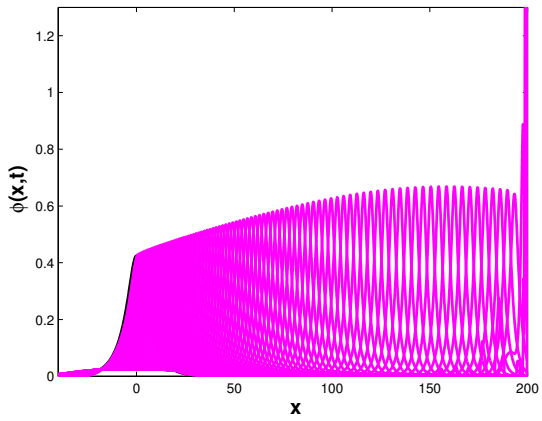

(d) $IC = 1.02$, longer x-axis

Figure 9: Simulations for $p = 5$ and $\tilde{C} = 1.00$, in (a) and (c) and $\tilde{C} = 1.02$, in (b) and (d). The initial condition is given in black. In figure (c) and (d), the x-interval is longer, though in all cases, the solution seems to blow up near the boundary of the domain. This is a numerically problem, though it is already known that the borderline case $p = 5$ is numerically very hard to solve, see [5]. However, it is also possible that the value of $\tilde{C}$ is too small to imply blow-up behaviour. Therefore, it would be interesting to study the case $p = 5$ numerically more thoroughly.

3 Dynamical rescaling

In this chapter, we derive the equation that we study in the rest of this thesis. In order to analyse solutions of equation (1.1) that blow up, we apply a dynamical rescaling. With this rescaling, we scale out the blow-up. The numerical simulations suggest the solutions to have a travelling structure and that the speed of the solution changes in time. The simulations also show a bump of which width scales with the blow-up. Therefore, we introduce the following dynamical rescaling

$$v(\xi,t) = L(t)^{\alpha}\phi(x,t) \text{ with } \xi = L^{-\beta}\left(x + cL^{\beta-\gamma}\right), \tag{3.1}$$

where $L(t) \to 0$ as $t \to T$ and α, β and γ positive constants. The term $cL^{\beta-\gamma}$ corresponds to the wave speed. Since the function $L(t)$ is explicitly a function of the variable t, the same holds for the function $v(\xi,t)$. Moreover, we assume v to be bounded, this indeed implies that ϕ blows up as the blow-up time T is approached. The ansatz (3.1) is substituted into equation (1.1). After multiplying with $L^{\alpha+3\beta}$ the equation becomes

$$-\frac{dL}{dt}L^{3\beta-\gamma-1}[-c(\beta-\gamma)v_{\xi}+L^{\gamma}(\alpha v+\beta\xi v_{\xi})]+v_{\xi\xi\xi}+\frac{1}{L^{(p-1)\alpha-2\beta}}(|v|^{p-1}v)_{\xi}+L^{3\beta}v_t=0. \tag{3.2}$$

Now, we study this equation as $t \to T$, therefore, L is small. In further analysis we view this as the small term. A significance degeneration is obtained when balancing the first, third, (the third-order derivative), and the fourth, (the non-linearity), term. The other terms are higher-order terms in L since $L \ll 1$. Balancing of the third-order derivative and the non-linear term gives the relation $\alpha = \frac{2\beta}{p-1}$. A balance with the first term is obtained by setting

$$\frac{dL}{dt}L(t)^{3\beta-\gamma-1} = -1. \tag{3.3}$$

Substituting these assumptions, equation (3.2) becomes

$$v_{\xi\xi\xi} + (v^p)_{\xi} - c(\beta-\gamma)v_{\xi} + L^{\gamma}\beta\left[\frac{2}{p-1}v + \xi v_{\xi}\right] + L^{3\beta}v_t = 0. \tag{3.4}$$

From now on, we study this equation where v is assumed to be bounded. Solving equation (3.3) by using separation of variables, we obtain

$$L(t) = ((3\beta-\gamma)(T-t))^{\frac{1}{3\beta-\gamma}}.$$

To fulfill the requirement that $L(t) \to 0$ as $t \uparrow T$, it is necessary to chooce

$$3\beta - \gamma > 0.$$

In the next sections we analyse the solution to equation (3.4) in different regions of ξ-values. We use $L \ll 1$ in the asymptotic analysis.

3.1 The bump region

In this section we study equation (3.4) for ξ around $\xi = 0$. From chapter 2, we assume the solution of the original equation (1.1) to have a bump occuring in this region, which is why we call it the bump region. The simulations show that this bump is blowing up as t approaches T. Therefore we study solutions that have a bump around $\xi = 0$. We assume the solution has a maximum at $\xi = 0$, thus, the condition $\frac{\partial v}{\partial \xi}|_{\xi=0} = 0$ is required.

As a first step, equation (3.4) is integrated with respect to ξ, resulting in

$$v_{\xi\xi} + v^p - dv + \mathcal{C} + L^\gamma \beta \left[\xi v + \frac{3-p}{p-1} \int^\xi v ds \right] + L^{3\beta} \int^\xi v_t \, ds = 0, \tag{3.5}$$

for some integration constant $\mathcal{C}$ and $d = c(\beta - \gamma)$.

To analyse equation (3.5) a regular asymptotic expansion is used

$$v = v_0 + L^\gamma v_1 + \text{h.o.t.} \tag{3.6}$$

Note that in the dynamical rescaling, in chapter 3, we assumed that $3\beta > \gamma$. Therefore, $L^{3\beta} \ll L^\gamma$, and thus, this is the correct expansion. Substitution into equation (3.4) leads to

$$v_{0_{\xi\xi}} + v_0^p - dv_0 + \mathcal{C} + L^\gamma \left[\beta \left(\xi v_0 + \frac{3-p}{p-1} \int^\xi v_0 \, ds \right) + v_{1,\xi\xi} + p v_0^{p-1} v_1 - d v_1 \right] + \text{h.o.t.} = 0 \tag{3.7}$$

As long as $L^\gamma \xi v_0 \ll v_0$ or in other words $\xi \ll L^{-\gamma}$, the leading order equation becomes

$$v_{0_{\xi\xi}} - dv_0 + v_0^p + \mathcal{C} = 0. \tag{3.8}$$

Therefore, the range of the bump region is defined to be $|\xi| \ll L^{-\gamma}$, see also figure 3.

First, we solve the homogeneous part of equation (3.8). This is a Hamiltonian equation with corresponding Hamiltonian $H(v_0, v_{0_\xi}) = \frac{1}{2} v_{0_\xi}^2 - \frac{1}{2} d v_0^2 + \frac{1}{p+1} v_0^{p+1}$. The solution we are interested in is the one corresponding to the homoclinic orbit in the (v_0, v_{0_ξ})-plane. The calculations therefor are given in appendix A and yield

$$v_0(\xi) = \left(\frac{d(p+1)}{2} \right)^{\frac{1}{p-1}} \operatorname{sech}^{\frac{2}{p-1}} \left(\frac{p-1}{2} \sqrt{d} \xi \right).$$

For negative d, the function would become a cosine-function, which is a bounded function but also oscillating, which is not what we consider, due to the conservation of mass. Therefore, we must choose $d > 0$. This condition implies, with $d = c(\beta - \gamma)$, that c and $\beta - \gamma$ must have the same sign. Note that this indeed corresponds to the numerical simulations performed in chapter 2. There, it is observed that the solution is moving to the right and that the speed increases as t approached the blow-up time. This first observation implies that c has to be negative. Moreover, the contribution of $cL^{\beta-\gamma}$ should become larger as $t \uparrow T$, and hence, we need $\beta < \gamma$. Thus, $\beta - \gamma < 0$ and $\beta - \gamma$ and c indeed have the same sign.

We are now interested in a particular solution v_0^* of equation (3.8). Since we are only interested in one particular solution we consider the case where $v_{0_{\xi\xi}} = 0$. Therefore a particular solution is a constant satisfying

$$(v_0^*)^p - dv_0^* + \mathcal{C} = 0.$$

Summarizing, we conclude that the leading order solution of equation (3.7) is given by

$$v_0(\xi) = \left(\frac{d(p+1)}{2}\right)^{\frac{1}{p-1}} \operatorname{sech}^{\frac{2}{p-1}}\left(\frac{p-1}{2}\sqrt{d}\xi\right) + v_0^*. \tag{3.9}$$

Now we look at the $\mathcal{O}(L^\gamma)$-terms in the expansion of the solution. The equation for v_1 reads:

$$v_{1,\xi\xi} - dv_1 + pv_0^{p-1}v_1 = -\beta\left[\frac{3-p}{p-1}\int^\xi v_0\, ds + \xi v_0\right] := g(\xi). \tag{3.10}$$

In appendix B we determine the function $g(\xi)$ explicitly, and it is given by

$$\begin{aligned} g(\xi) &= -\beta\frac{2(3-p)}{\sqrt{d}(p-1)^2}\left(\frac{d(p+1)}{2}\right)^{\frac{1}{p-1}}\sinh\left(\frac{p-1}{2}\sqrt{d}\xi\right) \\ &\quad \times \text{Hypergeometric2}F1\left[\frac{1}{2}, \frac{p+1}{2(p-1)}, \frac{3}{2}, -\sinh^2\left(\frac{p-1}{2}\sqrt{d}\xi\right)\right] \\ &\quad -\beta\xi\left(\frac{d(p+1)}{2}\right)^{\frac{1}{p-1}}\operatorname{sech}^{\frac{2}{p-1}}\left(\frac{p-1}{2}\sqrt{d}\xi\right), \end{aligned}$$

where the Hypergeometric function is given by

$$\text{Hypergeometric2F1}[a,b,c,z] = \sum_{n=0}^{\infty}\frac{(a)_n(b)_n}{(c)_n}\frac{z^n}{n!},$$

with $(d)_n$ the Pochhammer symbol.

Again, we first study the homogeneous equation

$$v_{1_{\xi\xi}} - dv_1 + pv_0^{p-1}v_1 = 0. \tag{3.11}$$

By differentiating equation (3.8) with respect to ξ, we can deduce that v_{0_ξ} is a solution to equation (3.11). Therefore a solution is

$$\begin{aligned} \psi_1(\xi) &= v_{0,\xi} \\ &= -\sqrt{d}\left(\frac{d(p+1)}{2}\right)^{\frac{1}{p-1}}\operatorname{sech}^{\frac{1+p}{p-1}}\left(\frac{(p-1)\sqrt{d}}{2}\xi\right)\sinh\left(\frac{(p-1)\sqrt{d}}{2}\xi\right), \end{aligned}$$

which is odd and exponentially decaying. Using the method of reduction of order, a second linear independent solution can be found. We determine it explicitly since we need the

expression in the following analysis. It is given by

$$\begin{aligned}\psi_2(\xi) &= \psi_1(\xi)\int^{\xi}\frac{ds}{(v_{0,s})^2}\\ &= -\frac{2(3+p)}{d(p-1)^2}\left(\frac{d(p+1)}{2}\right)^{-\frac{1}{p-1}}\sinh^2\left(\frac{p-1}{2}\sqrt{d}\xi\right)\operatorname{sech}^{1+\frac{2}{p-1}}\left(\frac{p-1}{2}\sqrt{d}\xi\right)\\ &\quad\times\text{Hypergeometric2}F1\left[\frac{1}{2},\frac{1}{2}-\frac{2}{p-1},\frac{3}{2},-\sinh^2\left(\frac{p-1}{2}\sqrt{d}\xi\right)\right]\\ &\quad+\frac{2}{d(p-1)}\left(\frac{d(p+1)}{2}\right)^{-\frac{1}{p-1}}\cosh^{\frac{2}{p-1}}\left(\frac{p-1}{2}\sqrt{d}\xi\right).\end{aligned}$$

This solution is even and exponentially growing. Finally, the general solution of equation (3.10) is constructed by using the method of variation of parameters as

$$v_1(\xi) = A_1\psi_1 + A_2\psi_2 - \psi_1\int_0^{\xi}\frac{\psi_2\ g}{W}ds + \psi_2\int_0^{\xi}\frac{\psi_1\ g}{W}ds.$$

Here, the constants A_1 and A_2 are still free to choose. Here, W is the Wronskian determinant which is equal to

$$\begin{aligned}W[\psi_1,\psi_2] &= \psi_1\ \frac{d\psi_2}{d\xi} - \frac{d\psi_1}{d\xi}\psi_2\\ &= 1.\end{aligned}$$

Then, the expression reduces to

$$v_1(\xi) = A_1\psi_1 + A_2\psi_2 - \psi_1\int_0^{\xi}\psi_2\ g\ ds + \psi_2\int_0^{\xi}\psi_1\ g\ ds. \tag{3.12}$$

In appendix B, expression (3.12) is evaluated for large ξ. We namely need to certify that expansion (3.6) remains a correct asymptotic expansion in the bump region. Since v_1 is exponentially growing and v_0 is exponentially decaying, we need to assume certain restrictions. In this analysis, we will take two different approaches, which are based on the approach taken for the Ginzburg-Landau equation in [14]. For this we need that $L^{\gamma}|v_1| \ll |v_0|$ for all ξ in the bump region. The first approach is by choosing the constant A_2 in a convenient way to fulfill this condition. The second approach to fulfill this condition is to redefine the bump region. Both approaches will give certain relations between the (so far) unknown parameters and constants. We postpone this analysis to the matching procedure in chapter 4.

To summarize the results of appendix B we find that both integrals converge to a constant for large $|\xi|$. Leaving out the first term, the asymptotic behaviour, for large $|\xi|$, of expression (3.12) is given by expression (C.11). For large $|\xi|$, this expression grows exponentially, depending on choices of parameters.

Recall that we assumed v to be a solution with a maximum at $\xi = 0$. From this condition, $\frac{\partial v_1}{\partial \xi}|_{\xi=} = 0$, the constant A_1 can be determined. The derivative of $v_1(\xi)$ is equal

to

$$v_{1_\xi} = A_1\psi_{1,\xi} + A_2\psi_{2,\xi} - \frac{d\psi_1}{d\xi}\int_0^\xi \psi_2\ g\ ds + \frac{d\psi_2}{d\xi}, \int_0^\xi \psi_1\ g\ ds$$

and evaluating this expression at $\xi = 0$ gives

$$v_{1_\xi}(0) = A_1\psi_{1,\xi}(0).$$

For this expression to be equal to zero, we choose $A_1 = 0$, since $\psi_{1,\xi} \neq 0$. The second constant A_2 will be determined in chapter 4.

Summarizing, the solution of equation (3.5) becomes

$$v(\xi) = v_0 + L^\gamma\left(\psi_2\left(A_2 + \int_0^\xi \psi_1\ g\ ds\right) - \psi_1\int_0^\xi \psi_2\ g\ ds\right) + \text{h.o.t.}, \tag{3.13}$$

where v_0 is given in (3.9).

3.2 The far field

In this section, we study solutions of equation (3.4) in the far field, so for $|\xi| \gg 1$. Numerical simulations suggest that $|v| \ll 1$ in this region. Hence we linearise around $v = 0$. Since $|\xi| \gg 1$, we introduce the rescaling

$$y = L^\sigma\xi, \quad \sigma > \gamma.$$

Note that for the choice $\gamma > \sigma$ this reduces to the bump region, studied in section 3.1.

Substituting this rescaling into equation (3.4) gives, after linearising,

$$L^{3\sigma}v_{yyy} - dL^\sigma v_y + L^\gamma\beta\left[\frac{2}{p-1}v + yv_y\right] + L^{3\beta}v_t = 0. \tag{3.14}$$

Since $\sigma > \gamma$ and $3\beta > \gamma$, the leading order part reads

$$\frac{2}{p-1}v + yv_y = 0. \tag{3.15}$$

This equation can be solved using the method of separation of variables. Thus the solution in the far field to the right of the bump region for $y > 0$, and hence $\xi > 0$, is denoted by

$$v_{ffright} = C_{ffright}\ y^{-\frac{2}{p-1}} = C_{ffright}\ (L^\sigma\xi)^{-\frac{2}{p-1}}, \tag{3.16}$$

and the solution to the left-hand side of the bump region for $y < 0$, and for $\xi < 0$, by

$$v_{ffleft} = C_{ffleft}\ |y|^{-\frac{2}{p-1}} = C_{ffleft}\ |L^\sigma\xi|^{-\frac{2}{p-1}}. \tag{3.17}$$

The solutions in the far field decay algebraically while the solution in the bump region has an exponentially decay. Consequently we can not match the two regions directly. Therefore, an intermediate region is introduced, where solutions to equation (1.1) are studied. The resulting equation is an third-order ordinary differential equation, for which the solutions are known. By determining the asymptotic behaviour for large ξ, the solution in the bump region is matched to the solutions in the far field through the solutions of the intermediate region.

3.3 The intermediate region

In this section we analyse the solutions to equation (3.4) in the intermediate region. By setting $\sigma = \frac{1}{3}\gamma$, we obtain a significance degeneration of equation (3.14)

$$v_{yyy} + \frac{2\beta}{p-1}v + \left(\beta y - dL^{-\frac{2}{3}\gamma}\right) v_y = 0. \tag{3.18}$$

We rewrite this equation in a more convenient way by introducing the rescaling

$$z = -\left(\frac{\beta}{4}\right)^{\frac{1}{3}} \left(y - \frac{d}{\beta}L^{-\frac{2\gamma}{3}}\right).$$

Then, equation (3.18) results in

$$v_{zzz} - 4zv_z - \frac{8}{p-1}v = 0. \tag{3.19}$$

There exists a turning point when the term in front of the first derivative of v changes sign. For (3.19) this happens at $z = 0$, which corresponds to

$$y = \frac{d}{\beta}L^{-\gamma}, \text{ and hence, to } \xi_{tp} = \frac{d}{\beta}L^{-\gamma}.$$

Note, since $d, \beta > 0$, that, $\xi_{tp} > 0$. At this point, the behaviour of the solution changes from elliptic on the left-hand side to parabolic on the right-hand side.

With the method used in [17], a general solution of equation (3.19) can be found. Suppose the solution looks like

$$v(z) = \int_C e^{zt} g(t)\ dt, \tag{3.20}$$

where $g(t)$ is an as yet as unknown function and C is a path in the complex plane to be determined once $g(t)$ is known. Substitution into equation (3.19) yields

$$\int_C t^3 g(t) e^{zt}\ dt - 4\int_C ztg(t)e^{zt}\ dt - \frac{8}{p-1}\int_C g(t)\ e^{zt}\ dt = 0. \tag{3.21}$$

Using integration by parts on the second term of (3.21), the third-order differential equation (3.19) is equivalent to the first-order differential equation

$$\int_C e^{zt}\left[g(t)\left(t^3 + \frac{4(p-3)}{p-1}\right) + 4t\frac{dg}{dt}\right] = 0 \tag{3.22}$$

with a boundary condition that

$$g(t)te^{zt} = 0 \text{ on the boundary of the path } C. \tag{3.23}$$

Solving equation (3.22) by using separation of variables gives us the function $g(t)$,

$$g(t) = De^{\frac{-t^3}{12}}\ t^{\frac{3-p}{p-1}},$$

where D is some constant. Thus, the term of the integral of (3.20) becomes

$$w(t) = e^{zt} g(t) = D e^{zt - \frac{1}{12}t^3} t^{\frac{3-p}{p-1}}. \tag{3.24}$$

The obvious choice for the path of integration, C, is a closed curve. However, since (3.24) is an entire function, we would get $v(z) = 0$ as a solution to equation (3.19). An open path with finite endpoints would violate condition (3.23). Hence, the end points, say a and b, of the contour must lie in the complex ∞-plane. Let $t = re^{i\theta}$. Then, for large t, function (3.24) reduces to

$$w(t) = D e^{-\frac{1}{12}r^3 \cos(3\theta)}.$$

To satisfy condition (3.23), we must have $w(t) \to 0$ as $t \to a, b$. Hence, a convenient choice is to let $r \to \infty$ and to choose $\cos(3\theta) = 1$, which implies $\theta = 0, \frac{2\pi}{3}, \frac{4\pi}{3}$. This choice corresponds to the paths, C_i, shown in figure 10(left). Any linear combination of these paths yields a solution to equation (3.19). In appendix D, the asymptotic expanions of the corresponding solutions are determined, for $z \to \pm\infty$. By splitting up the paths in figure 10(left) into the paths sketched in figure 10(right) and taking different combinations, three different asymptotic expressions are determined.

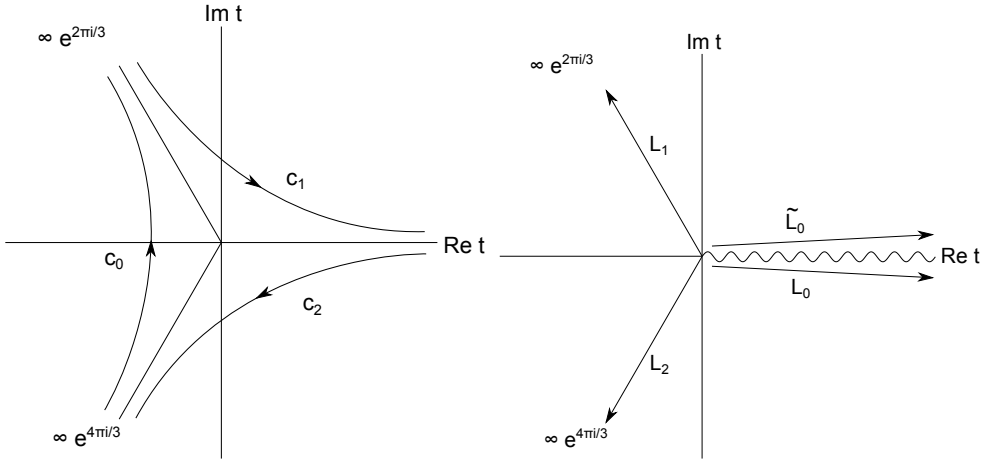

Figure 10: The integration paths C_i and L_i.

Summarizing, the solution to equation (3.19) to the right of the bump region, for $\xi < 0$, is given by

$$v_{IMR_{right}} = \sum_{i=0}^{2} c_i \int_{\Gamma_i} t^{\frac{3-p}{p-1}} e^{zt - \frac{1}{12}t^3} \, dt, \tag{3.25}$$

and to the left of the bump region, by

$$v_{IMR_{left}} = \sum_{i=0}^{1} d_i \int_{\Gamma_i} t^{\frac{3-p}{p-1}} e^{zt - \frac{1}{12}t^3} \, dt, \tag{3.26}$$

where c_i, d_i are constants. For convenience, we choose that paths Γ_i as follows

$$\begin{aligned} \Gamma_0 &= C_0, \\ \Gamma_1 &= L_1 + L_2, \\ \Gamma_2 &= C_2 - C_1. \end{aligned}$$

For $p = 5$, solutions to equation (3.19) are explicitly known, see expression [10.4.57] in [2]. For $p = 5$ equation (3.19) reduces to

$$v_{zzz} - 4zv_z - 2v = 0, \tag{3.27}$$

and the solutions to this equation are given by products of the Airy functions, A_i and B_i. Namely by A_i^2, B_i^2 and A_iB_i. Hence, for $p = 5$, the solutions (3.25) and (3.26) reduce to

$$v_{IMR_{right}} = c_0A_i^2 + c_1A_iB_i + c_2B_i^2 \tag{3.28}$$

and

$$v_{IMR_{left}} = d_0A_i^2 + d_1A_iB_i + d_2B_i^2. \tag{3.29}$$

The contours Γ_i are chosen such that the analysis presented above reduces for $p = 5$ to these products of Airy functions. See [13] for integral representations of these products of Airy functions which indeed correspond to our expressions.

4 Matching for p close to p = 5

In this chapter, we match the solution in the bump region to the solutions in the far field. We take p close to $p = 5$, since we then know the asymptotics of the solutions in the intermediate region. First, we analyse the region to the right-hand side of the bump region, where $\xi > 0$. The solution in the bump region is matched with the solution in the intermediate region and this is matched to the solution in the far field. A similar procedure will be done at the left-hand side of the bump region, where $\xi < 0$. See Figure 3 for the corresponding intervals.

4.1 Matching the solutions to the right of the bump region

We start with matching the solutions for $\xi > 0$ and $L^{\frac{\gamma}{3}}(\xi_{tp} - \xi) \gg 1$. The latter condition is needed since the asymptotics of the Airy-functions are only known for $|z| \gg 1$.

We start with matching the bump solution, (3.13), to the solution, (3.29), valid at the left-hand side of the turning point. In appendix D, the asymptotics of the Airy functions is given. The leading order term for $\xi \ll \xi_{tp}$ is given by

$$\begin{aligned} c_0 A_i^2 &= c_0 2^{-\frac{5}{3}} \pi^{-1} d^{-\frac{1}{2}} \beta^{\frac{1}{3}} L^{\frac{\gamma}{3}} e^{-\frac{2}{3} d^{\frac{3}{2}} \beta^{-1} L^{-\gamma}} + \cdots \\ c_1 A_i B_i &= c_1 2^{-\frac{2}{3}} \pi^{-1} d^{-\frac{1}{2}} \beta^{\frac{1}{3}} L^{\frac{\gamma}{3}} + \cdots \\ c_2 B_i^2 &= c_2 2^{\frac{1}{3}} \pi^{-1} d^{-\frac{1}{2}} \beta^{\frac{1}{3}} L^{\frac{\gamma}{3}} e^{\frac{2}{3} d^{\frac{3}{2}} \beta^{-1} L^{-\gamma} - \sqrt{d}\xi} + \cdots \end{aligned} \tag{4.1}$$

Evaluating the expressions (3.13) and (C.11) for $p = 5$, the asymptotic behaviour of the solution in the bump region is given by

$$v_0(\xi) = (3d)^{\frac{1}{4}} \sqrt{2} e^{-\sqrt{d}\xi} + v_0^* - L^{\gamma} A_2 \frac{1}{2\sqrt{2} d (3d)^{\frac{1}{4}}} e^{\sqrt{d}\xi}. \tag{4.2}$$

Both the first term of expression (4.2) and the last term in (4.1) are exponentially decaying, therefore, these two terms have to be matched with each other. The $A_i B_i$-term is a constant, just like v_0^*, hence, these two terms are matched as well. The contribution of A_i^2 is exponentially small, therefore, c_0 remains free to be chosen. To ensure that expression (3.6) remains an asymptotic expansion in the bump region, we choose $A_2 = 0$. Another approach would be to let A_2 undetermined and redefine the bump region. As long as $L^{\gamma}|v_1| \ll |v_0|$, or $|\xi| \ll \frac{\log(CL^{-\gamma})}{2\sqrt{d}}$, with C a constant of order $\mathcal{O}(1)$, epxression (3.6) remains an asymptotic expansion in the bump region.

In order to match the bump solution (3.13) to the solution (3.28) valid at the right-hand side of the turning point, we choose

$$\begin{aligned} c_2 &= (3d)^{\frac{1}{4}} 2^{\frac{1}{6}} \pi d^{\frac{1}{2}} \beta^{-\frac{1}{3}} L^{-\frac{\gamma}{3}} e^{-\frac{2}{3} d^{\frac{3}{2}} \beta^{-1} L^{-\gamma}}, \\ v_0^* &= c_1 2^{-\frac{2}{3}} \pi^{-1} d^{-\frac{1}{2}} \beta^{\frac{1}{3}} L^{\frac{\gamma}{3}}, \\ A_2 &= 0. \end{aligned}$$

Now we match the solution in the intermediate region to the solution in the far field, (3.16), for $\xi \gg \xi_{tp}$. There, the asymptotic expansions of the Airy-functions are given, see appendix D, by

$$\begin{aligned} c_0 A_i^2 &= c_0 \pi^{-1} \left(\tfrac{\beta}{4}\right)^{-\frac{1}{6}} L^{-\frac{\gamma}{6}} (\xi_{tp} - \xi)^{-\frac{1}{2}} \sin^2\left(\tilde{\xi}\right) + \cdots \\ c_1 A_i B_i &= c_1 \pi^{-1} \left(\tfrac{\beta}{4}\right)^{-\frac{1}{6}} L^{-\frac{\gamma}{6}} (\xi_{tp} - \xi)^{-\frac{1}{2}} \sin\left(\tilde{\xi}\right)\cos\left(\tilde{\xi}\right) \cdots \\ c_2 B_i^2 &= c_2 \pi^{-1} \left(\tfrac{\beta}{4}\right)^{-\frac{1}{6}} L^{-\frac{\gamma}{6}} (\xi_{tp} - \xi)^{-\frac{1}{2}} \cos^2\left(\tilde{\xi}\right) \cdots \end{aligned} \tag{4.3}$$

where $\tilde{\xi} = \left(\frac{\beta}{4}\right)^{\frac{1}{3}} L^{\frac{\gamma}{3}} (\xi_{tp} - \xi) + \frac{\pi}{4}$.

The solution (3.28) can be rewritten in a more convenient way, as

$$\begin{aligned} v_{WKBJ_{right}} &= \pi^{-1} \left(\frac{\beta}{4} L^{\gamma}\right)^{-\frac{1}{6}} \xi^{-\frac{1}{2}} \cdot \\ &\quad \left[\frac{c_0}{2}\left(1 - \cos\left(2\tilde{\xi}\right)\right) + \frac{c_1}{2}\sin\left(2\tilde{\xi}\right) + \frac{c_2}{2}\left(1 + \cos\left(2\tilde{\xi}\right)\right)\right]. \end{aligned} \tag{4.4}$$

The conservation of mass, (1.2), implies that the solution is not oscillating, and therefore we choose $c_1 = 0$ and $c_0 = c_2$. Then, expression (4.4) reduces to

$$v_{WKBJ_{right}} = c_2 \pi^{-1} \left(\frac{\beta}{4} L^{\gamma}\right)^{-\frac{1}{6}} \xi^{-\frac{1}{2}}.$$

The solution in the far field is given by

$$v_{ff_{right}} = C_{ff_{right}} L^{-\frac{\gamma}{6}} \xi^{-\frac{1}{2}}.$$

So by choosing

$$C_{ff_{right}} = c_2 2^{\frac{2}{3}} \pi^{-1} \beta^{-\frac{1}{6}},$$

the two solutions are perfectly matched to each other. Note that in matching the solutions in the intermediate region and the far field, a condition on the solution in the bump region is used. Since we have chosen $c_1 = 0$, the function v_0^* has to be equal to $v_0^* = 0$.

4.2 Matching the solutions to the left of the bump region

In this section, the solutions for $\xi < 0$ will be matched. We start by matching the solution in the bump region, (3.13), with the solution in the intermediate region, (3.29). The leading order of the various terms of the solution (3.29) is given by

$$\begin{aligned} d_0 A_i^2 &= d_0 2^{-\frac{5}{3}} \pi^{-1} d^{-\frac{1}{2}} \beta^{\frac{1}{3}} L^{\frac{\gamma}{3}} e^{-\frac{2}{3} d^{\frac{3}{2}} \beta^{-1} L^{-\gamma} - \sqrt{d}|\xi|} + \cdots \\ d_1 A_i B_i &= d_1 2^{-\frac{2}{3}} \pi^{-1} d^{-\frac{1}{2}} \beta^{\frac{1}{3}} L^{\frac{\gamma}{3}} + \cdots \\ d_2 B_i^2 &= d_2 2^{\frac{1}{3}} \pi^{-1} d^{-\frac{1}{2}} \beta^{\frac{1}{3}} L^{\frac{\gamma}{3}} e^{\frac{2}{3} d^{\frac{3}{2}} \beta^{-1} L^{-\gamma}} + \cdots \end{aligned} \tag{4.5}$$

Evaluating the expressions (3.13) and (C.11) for $p = 5$, the asymptotic behaviour of the solution in the bump region is given by

$$v_0(\xi) = (3d)^{\frac{1}{4}} \sqrt{2} e^{-\sqrt{d}|\xi|} + v_0^* + L^{\gamma} \left[\frac{\pi \beta (3d)^{\frac{1}{4}}}{4d\sqrt{d}} \frac{\Gamma\left(\frac{1}{4}\right)}{\Gamma\left(\frac{3}{4}\right)} - A_2 \frac{1}{2\sqrt{2} d (3d)^{\frac{1}{4}}} e^{\sqrt{d}\xi}\right] + \cdots \tag{4.6}$$

In section 4.1, the matching procedure yielded

$$\begin{aligned} v_0^* &= 0 \\ A_2 &= 0 \end{aligned}$$

Thus, expression (4.6) reduces to

$$v_0(\xi) = (3d)^{\frac{1}{4}}\sqrt{2}e^{-\sqrt{d}|\xi|} + L^{\gamma}\frac{\pi\beta(3d)^{\frac{1}{4}}}{4d\sqrt{d}}\frac{\Gamma\left(\frac{1}{4}\right)}{\Gamma\left(\frac{3}{4}\right)} + \cdots \tag{4.7}$$

Note that the B_i^2-term in (4.5) is exponentially growing. Since there are no terms in the bump region which have a similar behaviour, this term has to be cancelled. Both the A_i^2-term in (4.5) and the first term in (4.7) are exponentially decaying, therefore, these two terms are matched to each other. The remaining two terms are both constants and are, thus, also matched together.

Therefore, in order to match the bump solution (3.13) with the solution (3.29) valid at the left-hand side of the bump region, we choose

$$\begin{aligned} d_0 &= (3d)^{\frac{1}{4}}2^{\frac{13}{6}}\pi^1 d^{\frac{1}{2}}\beta^{-\frac{1}{3}}L^{-\frac{\gamma}{3}}e^{\frac{2}{3}d^{\frac{3}{2}}\beta^{-1}L^{-\gamma}}, \\ L^{\gamma}\frac{\pi\beta(3d)^{\frac{1}{4}}}{4d\sqrt{d}}\frac{\Gamma\left(\frac{1}{4}\right)}{\Gamma\left(\frac{3}{4}\right)} &= d_1 2^{-\frac{2}{3}}\pi^{-1}d^{-\frac{1}{2}}\beta^{\frac{1}{3}}L^{\frac{\gamma}{3}}, \\ d_2 &= 0. \end{aligned}$$

Finally, we match the solution valid in the intermediate region, (3.29) with the solution valid in the far field, (3.17). For $|\xi| \gg L^{-\gamma}$, the asymptotic expansions of the various terms of solution (3.29) are given by

$$\begin{aligned} d_0A_i^2 &= d_0 2^{-\frac{5}{3}}\pi^{-1}\beta^{-\frac{1}{6}}L^{-\frac{\gamma}{6}}|\xi|^{-\frac{1}{2}}e^{-\frac{2}{3}d^{\frac{3}{2}}\beta^{-1}L^{-\gamma}-\sqrt{d}|\xi|} + \cdots \\ d_1A_iB_i &= d_1 2^{-\frac{2}{3}}\pi^{-1}d^{-\frac{1}{2}}\beta^{-\frac{1}{6}}L^{-\frac{\gamma}{6}}\,|\xi|^{-\frac{1}{2}} \\ d_2B_i^2 &= d_2 2^{\frac{1}{3}}\pi^{-1}\beta^{-\frac{1}{6}}L^{-\frac{\gamma}{6}}|\xi|^{-\frac{1}{2}}e^{\frac{2}{3}d^{\frac{3}{2}}\beta^{-1}L^{-\gamma}+\sqrt{d}|\xi|} + \cdots \end{aligned} \tag{4.8}$$

The solution in the far field is given by

$$v_{ffleft} = C_{ffleft}|\xi|^{-\frac{1}{2}}L^{-\frac{\gamma}{6}}.$$

Althoug the B_i^2-term is dominating, the choice $d_2 = 0$ implies that for $|\xi| \gg L^{-\gamma}$, the solution in the intermediate region is dominated by the A_iB_i-term. This term is algebraically decaying and so is the solution in the far field. Therefore, the far field solution, (3.17), is matched to the solution valid in the intermediate region, (3.29), by choosing

$$C_{ffleft} = d_1 2^{-\frac{2}{3}}\pi^{-1}\beta^{-\frac{1}{6}}.$$

4.3 Summary

Summarizing the analysis, we have contructed a real leading order solution $\phi(\xi, t)$ for equation (1.1). The results we obtained so far are summarized in a sketch of the solution, found by the matching procedure of chapter 4 for p close to $p = 5$, see figure 11. Note that there is faster decay on the right-hand side of the bump region than on the left-hand side. This structure has also been observed in the numerical simulations, in chapter 2. All constants belonging to the solutions in the three different region of figure 3 are now expressed in terms of d, β and L^γ.

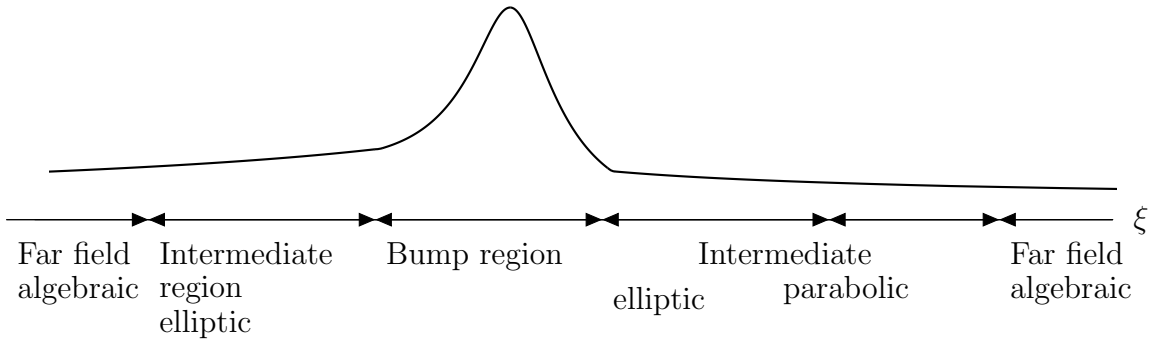

Figure 11: A sketch of the constructed solution to equation (1.1) for $p = 5$. There is a stronger decay on the right-hand side of the bump compared to the left-hand side. The solution is qualitatively drawn, though after the matching procedure, all the various constants are now expressed in terms of d, β and L^γ.

A logical next step would be to match the solutions of the bump region to the solutions in the far field, using the solutions in the interemediate region, for general $p > 5$. In chapter 3, the solutions founded in the various regions are valid for all p. We started with the determination of the asymptotic behaviour for large $|\xi|$ of the solutions in the intermediate region, see appendix D, but this is something to finish.

A Appendix: determining the expression of v_0

We study the equation

$$v_{0_{\xi\xi}} - dv_0 + v^p = 0.$$

Multiplying this equation with v_{0_ξ} and integrating by ξ results in the Hamiltonian function

$$H(v_0, v_{0_\xi}) = \frac{1}{2}v_{0_\xi}^2 - \frac{1}{2}dv_0^2 + \frac{1}{p+1}v_0^{p+1}.$$

We are interested in a solution with a maximum. This solution corresponds to the homoclinic orbit in the (v_0, v_{0_ξ})-plane. There are two fixed points $(v_0, v_{0_\xi}) = (0, 0)$, which is a saddle-point and $(v_0, v_{0_\xi}) = (0, 0)$, which is a centre. Since there is only one saddle-point, the homoclinic orbit has to be connected with the origin. Because $H(0, 0) = 0$, the Hamiltonian function for the solution we are interested in is equal to zero. The resulting equation is solved by using separation of variables.

$$\begin{aligned}
\frac{1}{2}v_{0_\xi}^2 - \frac{1}{2}dv_0^2 + \frac{1}{p+1}v_0^{p+1} &= 0 \\
\frac{dv_0}{d\xi} &= \pm v_0\sqrt{d - \frac{2}{p+1}v^{p-1}} \\
\frac{dv}{v_0\sqrt{d - \frac{2}{p+1}v_0^{p+1}}} &= \pm d\xi
\end{aligned}$$

Substitution of $w^2 = \frac{d(p+1)}{2}v_0^{1-p}$ with $dv_0 = \frac{4}{d(p+1)(1-p)}wv^p dw$ gives us

$$\begin{aligned}
\frac{2}{\sqrt{d}(1-p)}\int\frac{dw}{w^2-1} &= \int \pm d\xi \\
\frac{2}{\sqrt{d}(1-p)}\operatorname{arccosh}(w) &= \pm\xi \\
\operatorname{arccosh}(w) &= \pm\frac{p-1}{2}\xi \\
w(\xi) &= \cosh\left(\frac{p-1}{2}\sqrt{d}\xi\right) \\
\sqrt{\frac{d(p+1)}{2}}v_0^{\frac{1-p}{2}} &= \cosh\left(\frac{p-1}{2}\sqrt{d}\xi\right) \\
v_0(\xi) &= \left(\frac{d(p+1)}{2}\right)^{\frac{1}{p-1}}\operatorname{sech}^{\frac{2}{p-1}}\left(\frac{p-1}{2}\sqrt{d}\xi\right)
\end{aligned}$$

B Appendix: determining the solutions ψ_2 and g

We are interested in the behaviour of expression (3.13) for large ξ. Therefore, we need to determine the functions $\psi_2(\xi)$ and $g(\xi)$ of (3.12) explicitly. We start with the function $\psi_2(\xi)$, where we need the following expressions

$$
\begin{aligned}
v_{0_\xi} &= -\sqrt{d}\left(\frac{d(p+1)}{2}\right)^{\frac{1}{p-1}} \operatorname{sech}^{1+\frac{2}{p-1}}\left(\frac{p-1}{2}\sqrt{d}\xi\right)\sinh\left(\frac{p-1}{2}\sqrt{d}\xi\right)\\
\int_0^\xi \frac{ds}{(v_{0_s})^2} &= \left(\frac{d(p+1)}{2}\right)^{-\frac{2}{p-1}}\int_0^\xi d^{-1}\operatorname{sech}^{-2-\frac{4}{p-1}}\left(\frac{p-1}{2}\sqrt{d}\xi\right)\sinh^{-2}\left(\frac{p-1}{2}\sqrt{d}\xi\right)\,ds\\
&= d^{-1}\left(\frac{d(p+1)}{2}\right)^{-\frac{2}{p-1}}\int_0^\xi \operatorname{sech}^{-\frac{4}{p-1}}\left(\frac{p-1}{2}\sqrt{d}\xi\right)\,ds\\
&\quad +d^{-1}\left(\frac{d(p+1)}{2}\right)^{-\frac{2}{p-1}}\int_0^\xi \operatorname{sech}^{-\frac{4}{p-1}}\left(\frac{p-1}{2}\sqrt{d}\xi\right)\operatorname{csch}^2\left(\frac{p-1}{2}\sqrt{d}\xi\right)\,ds\\
&= \frac{2}{d\sqrt{d}(p-1)}\left(\frac{d(p+1)}{2}\right)^{-\frac{2}{p-1}}\sinh\left(\frac{p-1}{2}\sqrt{d}\xi\right)\\
&\quad \times\text{Hypergeometric2}F1\left[\frac{1}{2},\frac{p-5}{2(p-1)},\frac{3}{2},-\sinh^2\left(\frac{p-1}{2}\sqrt{d}\xi\right)\right]\\
&\quad +\left(\frac{d(p+1)}{2}\right)^{-\frac{2}{p-1}}\frac{8}{d\sqrt{d}(p-1)^2}\sinh\left(\frac{p-1}{2}\sqrt{d}\xi\right)\\
&\quad \times\text{Hypergeometric2}F1\left[\frac{1}{2},\frac{p-5}{2(p-1)},\frac{3}{2},-\sinh^2\left(\frac{p-1}{2}\sqrt{d}\xi\right)\right]\\
&\quad -\left(\frac{d(p+1)}{2}\right)^{-\frac{2}{p-1}}\frac{2}{d\sqrt{d}(p-1)}\cosh^{\frac{4}{p-1}+1}\left(\frac{p-1}{2}\sqrt{d}\xi\right)\operatorname{csch}\left(\frac{p-1}{2}\sqrt{d}\xi\right)
\end{aligned}
$$

Here, the Hypergeometric function is given by

$$\text{Hypergeometric2F1}[a,b,c,z]=\sum_{n=0}^{\infty}\frac{(a)_n(b)_n}{(c)_n}\frac{z^n}{n!},$$

with $(d)_n$ the Pochhammer symbol.

Thus the solution $\psi_2(\xi)$ is given by

$$
\begin{aligned}
\psi_2(\xi) &= \psi_1(\xi)\int^\xi \frac{ds}{(v_{0,s})^2}\\
&= -\frac{2(3+p)}{d(p-1)^2}\left(\frac{d(p+1)}{2}\right)^{-\frac{1}{p-1}}\sinh^2\left(\frac{p-1}{2}\sqrt{d}\xi\right)\operatorname{sech}^{1+\frac{2}{p-1}}\left(\frac{p-1}{2}\sqrt{d}\xi\right)\\
&\quad \times\text{Hypergeometric2}F1\left[\frac{1}{2},\frac{p-5}{2(p-1)},\frac{3}{2},-\sinh^2\left(\frac{p-1}{2}\sqrt{d}\xi\right)\right]\\
&\quad +\frac{2}{d(p-1)}\left(\frac{d(p+1)}{2}\right)^{-\frac{1}{p-1}}\cosh^{\frac{2}{p-1}}\left(\frac{p-1}{2}\sqrt{d}\xi\right). \qquad \text{(B.1)}
\end{aligned}
$$

To determine the function $g(\xi)$, the following expression is needed

$$\begin{aligned}\int_0^\xi v_0\, ds &= \left(\frac{d(p+1)}{2}\right)^{\frac{1}{p-1}} \int_0^\xi \operatorname{sech}^{\frac{2}{p-1}}\left(\frac{p-1}{2}\sqrt{d}\xi\right)\, ds \\ &= \frac{2}{\sqrt{d}(p-1)}\left(\frac{d(p+1)}{2}\right)^{\frac{2}{p-1}} \operatorname{sech}^{\frac{2}{p-1}}\left(\frac{p-1}{2}\sqrt{d}\xi\right)\sinh\left(\frac{p-1}{2}\sqrt{d}\xi\right) \\ &\quad \times \text{Hypergeometric}2F1\left[\frac{1}{2}, \frac{p+1}{2(p-1)}, \frac{3}{2}, -\sinh^2\left(\frac{p-1}{2}\sqrt{d}\xi\right)\right].\end{aligned}$$

Therefore, the function $g(\xi)$ becomes

$$\begin{aligned}g(\xi) &= -\beta\frac{2(3-p)}{\sqrt{d}(p-1)^2}\left(\frac{d(p+1)}{2}\right)^{\frac{1}{p-1}}\sinh\left(\frac{p-1}{2}\sqrt{d}\xi\right) \\ &\quad \times \text{Hypergeometric}2F1\left[\frac{1}{2}, \frac{p+1}{2(p-1)}, \frac{3}{2}, -\sinh^2(\frac{p-1}{2}\sqrt{d}\xi)\right] \\ &\quad -\beta\xi\left(\frac{d(p+1)}{2}\right)^{\frac{1}{p-1}}\operatorname{sech}^{\frac{2}{p-1}}\left(\frac{p-1}{2}\sqrt{d}\xi\right). \qquad \text{(B.2)}\end{aligned}$$

C Appendix: integrals bump region

To be able to determine the constants in solution (3.1) in the matching procedure, the expression of the two integrals in (3.12) as $|\xi| \to \infty$ are needed.

The integral $\int_0^\xi \psi_2 \; g \; ds$ will not be determined explicitly, but we use the asymptotic expansion of the integrand for large ξ. Then we integrate that expression before we multiply it with the asymptotic expression for large $|\xi|$ of the function ψ_1. This approach yield that the term $\psi_1 \int^\xi \psi_2 \; g \; ds$ converges to some constant, which we will explicitly determine, as $\xi \to \pm\infty$.

The integral $\psi_2 \int_0^\xi \psi_1 \; g \; ds$ can be determined explicitly. Also this integral converges to some constant, which will be determined, as $\xi \to \pm\infty$.

C.1 First integral

First the integral $\int_0^\xi \psi_1 \; g \; ds$ is calculated as

$$\begin{aligned}
\int_0^\xi \psi_1 \; g \; ds &= \int_0^\xi -\beta \; \frac{3-p}{p-1} \; v_{0,\xi} \int_0^s v_0 \; dr \; ds - \int_0^\xi \beta \; s \; v_0 \; v_{0,s} \; ds, \\
&= -\beta \; \frac{3-p}{p-1} \left[\left| v_0 \int_0^s v_0 \; dr \right|^\xi - \int_0^\xi v_0^2 \; ds \right] \\
&\quad -\beta \; \left[\left| \frac{1}{2} s \; v_0^2 \right|^\xi - \frac{1}{2} \int_0^\xi v_0^2 \; ds \right], \\
&= -\beta \; \left[\frac{3-p}{p-1} \; v_0 \int_0^s v_0 \; dr \right|^\xi + \frac{1}{2} \; s \; v_0 \Big|^\xi - \left(\frac{3-p}{p-1} + \frac{1}{2} \right) \int_0^\xi v_0^2 \; ds \Bigg], \\
&= -\beta \; \left[\frac{3-p}{p-1} v_0 \int_0^\xi v_0 \; ds + \frac{1}{2} \xi \; v_0^2 + \frac{p-5}{2(p-1)} \int_0^\xi v_0^2 \; ds \right],
\end{aligned}$$

where

$$\begin{aligned}
v_0 \int_0^\xi v_0 \; ds &= \frac{2}{\sqrt{d}(p-1)} \left(\frac{d(p+1)}{2} \right)^{\frac{2}{p-1}} \operatorname{sech}^{\frac{2}{p-1}} \left(\frac{p-1}{2} \sqrt{d} \; \xi \right) \\
&\quad \times \sinh \left(\frac{p-1}{2} \sqrt{d} \; \xi \right) \\
&\quad \times \text{Hypergeometric2F1} \left[\frac{1}{2}, \frac{p+1}{2(p-1)}, \frac{3}{2}, -\sinh^2 \left(\frac{p-1}{2} \sqrt{d} \; \xi \right) \right], \\
\xi \; v_0^2 &= \left(\frac{d(p+1)}{2} \right)^{\frac{2}{p-1}} \xi \; \operatorname{sech}^{\frac{4}{p-1}} \left(\frac{p-1}{2} \sqrt{d} \; \xi \right),
\end{aligned}$$

$$\int_0^\xi v_0^2 = \frac{2}{\sqrt{d}(p-1)}\left(\frac{d(p+1)}{2}\right)^{\frac{2}{p-1}}\sinh\left(\frac{p-1}{2}\sqrt{d}\,\xi\right) \times\text{Hypergeometric2F1}\left[\frac{1}{2},\frac{p+3}{2(p-1)},\frac{3}{2},-\sinh^2\left(\frac{p-1}{2}\sqrt{d}\,\xi\right)\right].$$

Thus the term $\psi_2\int_0^\xi \psi_1\, g\, ds$ is given by

$$\begin{aligned}
&\psi_2\int_0^\xi \psi_1\, g\, ds\\
=\;& \frac{4\beta(3+p)(3-p)}{d\sqrt{d}(p-1)^4}\left(\frac{d(p+1)}{2}\right)^{\frac{1}{p-1}}\sinh^2\left(\frac{p-1}{2}\sqrt{d}\,\xi\right)\operatorname{sech}^{\frac{4}{p-1}}\left(\frac{p-1}{2}\sqrt{d}\,\xi\right)\\
&\times\tanh\left(\frac{p-1}{2}\sqrt{d}\,\xi\right)\text{Hypergeometric2F1}\left[\frac{1}{2},\frac{p+1}{2(p-1)},\frac{3}{2},-\sinh^2\left(\frac{p-1}{2}\sqrt{d}\,\xi\right)\right]\\
&\times\text{Hypergeometric2F1}\left[\frac{1}{2},\frac{p-5}{2(p-1)},\frac{3}{2},-\sinh^2\left(\frac{p-1}{2}\sqrt{d}\,\xi\right)\right]\\
&+\frac{\beta(3+p)}{d(p-1)^2}\left(\frac{d(p+1)}{2}\right)^{\frac{1}{p-1}}\xi\sinh\left(\frac{p-1}{2}\sqrt{d}\,\xi\right)\operatorname{sech}^{\frac{6}{p-1}}\left(\frac{p-1}{2}\sqrt{d}\,\xi\right)\\
&\times\tanh\left(\frac{p-1}{2}\sqrt{d}\,\xi\right)\text{Hypergeometric2F1}\left[\frac{1}{2},\frac{p-5}{2(p-1)},\frac{3}{2},-\sinh^2\left(\frac{p-1}{2}\sqrt{d}\,\xi\right)\right]\\
&+\frac{2\beta(p+3)(p-5)}{d\sqrt{d}(p-1)^4}\left(\frac{d(p+1)}{2}\right)^{\frac{1}{p-1}}\sinh^2\left(\frac{p-1}{2}\sqrt{d}\,\xi\right)\operatorname{sech}^{\frac{2}{p-1}}\left(\frac{p-1}{2}\sqrt{d}\,\xi\right)\\
&\times\tanh\left(\frac{p-1}{2}\sqrt{d}\,\xi\right)\text{Hypergeometric2F1}\left[\frac{1}{2},\frac{p+3}{2(p-1)},\frac{3}{2},-\sinh^2\left(\frac{p-1}{2}\sqrt{d}\,\xi\right)\right]\\
&\times\text{Hypergeometric2F1}\left[\frac{1}{2},\frac{p-5}{2(p-1)},\frac{3}{2},-\sinh^2\left(\frac{p-1}{2}\sqrt{d}\,\xi\right)\right]\\
&-\frac{4\beta(3-p)}{d\sqrt{d}(p-1)^3}\left(\frac{d(p+1)}{2}\right)^{\frac{1}{p-1}}\sinh\left(\frac{p-1}{2}\sqrt{d}\,\xi\right)\\
&\times\text{Hypergeometric2F1}\left[\frac{1}{2},\frac{p+1}{2(p-1)},\frac{3}{2},-\sinh^2\left(\frac{p-1}{2}\sqrt{d}\,\xi\right)\right]\\
&-\frac{\beta}{d(p-1)^2}\left(\frac{d(p+1)}{2}\right)^{\frac{1}{p-1}}\xi\operatorname{sech}^{\frac{2}{p-1}}\left(\frac{p-1}{2}\sqrt{d}\,\xi\right)\\
&-\frac{2\beta(p-5)}{d\sqrt{d}(p-1)^3}\left(\frac{d(p+1)}{2}\right)^{\frac{1}{p-1}}\cosh^{\frac{2}{p-1}}\left(\frac{p-1}{2}\sqrt{d}\,\xi\right)\sinh\left(\frac{p-1}{2}\sqrt{d}\,\xi\right)\\
&\times\text{Hypergeometric2F1}\left[\frac{1}{2},\frac{p+3}{2(p-1)},\frac{3}{2},-\sinh^2\left(\frac{p-1}{2}\sqrt{d}\,\xi\right)\right].
\end{aligned}$$

We are interested in the asymptotics of this expression for large ξ. From the asymptotic expression [15.3] in [2], we know that

$$\begin{aligned}\text{Hypergeometric2F1}[a,b,c,z] &= \frac{\Gamma(b-a)\Gamma(c)}{\Gamma(b)\Gamma(c-a)}(-z)^{-a}\left(1+\frac{a(1+a-c)}{(1+a-b)z}+\cdots\right) &\text{(C.1)}\\ &+ \frac{\Gamma(a-b)\Gamma(c)}{\Gamma(a)\Gamma(c-b)}(-z)^{-b}\left(1+\frac{b(1+b-c)}{(1-a+b)z}+\cdots\right) &\text{(C.2)}\end{aligned}$$

as $|z|\to\infty \wedge a-b\notin\mathbb{Z}$.

Therefore, as $\xi\to\pm\infty$, the asymptotics of the term $\psi_2\left(A_2+\int_0^\xi \psi_1\ g\ ds\right)$ is given by

$$\begin{aligned}&\psi_2\left(A_2+\int_0^\xi \psi_1\ g\ ds\right)= &\text{(C.3)}\\ &e^{\sqrt{d}|\xi|}2^{-\frac{2}{p-1}}\left[\frac{\beta\sqrt{\pi}(p-5)}{2\sqrt{d}(p-1)^2}\frac{\Gamma\left(\frac{2}{p-1}\right)}{\Gamma\left(\frac{p+3}{2(p-1)}\right)}-A_2\left(\frac{d(p+1)}{2}\right)^{-\frac{2}{p-1}}\right]\\ &\times\left\{(\pm1)^{\frac{4}{p-1}}\frac{3+p}{d(p-1)^2}\frac{\Gamma\left(\frac{2}{p-1}\right)}{\Gamma\left(\frac{p+1}{p-1}\right)}\left(\frac{d(p+1)}{2}\right)^{\frac{1}{p-1}}\mp\frac{2}{d(p-1)}\left(\frac{d(p+1)}{2}\right)^{\frac{1}{p-1}}\right\}\\ &\mp\frac{\sqrt{\pi}\beta(p-3)}{d\sqrt{d}(p-1)^3}\left(\frac{d(p+1)}{2}\right)^{\frac{1}{p-1}}\frac{\Gamma\left(\frac{1}{p-1}\right)}{\Gamma\left(\frac{p+1}{2(p-1)}\right)}\left[\frac{3+p}{p-1}\frac{\Gamma\left(\frac{2}{p-1}\right)}{\Gamma\left(\frac{p+1}{p-1}\right)}-(\pm1)^{\frac{4}{p-1}}2\right]+\text{h.o.t.}\end{aligned}$$

C.2 Second integral

Now we analyse the second integral $\psi_1 \int^\xi \psi_2 \; g \; ds$. First, we determine the asymptotic expression for large ξ of the function ψ_1, which is given by (3.12). Second, we use the asymptotic expression of (C.1) to determine the asymptotic behaviour for large ξ of the integrand. At last we integrate the latter expression and multiply with the former to obtain the asymptotic behaviour of the whole term.

As $\xi \to \pm\infty$, the asymptotics of the function ψ_1 is given by

$$\psi_1(\xi) = -\sqrt{d}\left(\frac{d(p+1)}{2}\right)^{\frac{1}{p-1}} 2^{\frac{2}{p-1}} e^{-\sqrt{d}|\xi|}. \tag{C.4}$$

Using expressions (B.1) and (B.2), the integral $\int^\xi \psi_2 \; g \; ds$ is given by

$$\begin{aligned}
\int^\xi \psi_2 \; g \; ds \;\; = \;\; & -\frac{4\beta(p-3)(p+3)}{d\sqrt{d}(p-1)^4} \int^\xi \sinh^3\left(\frac{p-1}{2}\sqrt{d}\; s\right) \operatorname{sech}^{1+\frac{2}{p-1}}\left(\frac{p-1}{2}\sqrt{d}\; s\right) \\
& \times \mathrm{H2F1}\left[\frac{1}{2}, \frac{1}{2}\left(1-\frac{4}{p-1}\right), \frac{3}{2}, -\sinh^2\left(\frac{p-1}{2}\sqrt{d}\; s\right)\right] \\
& \times \mathrm{H2F1}\left[\frac{1}{2}, \frac{1}{2}\left(1+\frac{2}{p-1}\right), \frac{3}{2}, -\sinh^2\left(\frac{p-1}{2}\sqrt{d}\; s\right)\right] \; ds \\
& + \frac{4\beta(p-3)}{d\sqrt{d}(p-1)^3} \int^\xi \cosh^{\frac{2}{p-1}} \sinh\left(\frac{p-1}{2}\sqrt{d}\; s\right) \left(\frac{p-1}{2}\sqrt{d}\; s\right) \\
& \times \mathrm{H2F1}\left[\frac{1}{2}, \frac{1}{2}\left(1+\frac{2}{p-1}\right), \frac{3}{2}, -\sinh^2\left(\frac{p-1}{2}\sqrt{d}\; \xi\right)\right] \; ds \\
& + \frac{2\beta(p+3)}{d(p-1)^2} \int^\xi s \; \sinh^2\left(\frac{p-1}{2}\sqrt{d}\; s\right) \operatorname{sech}^{1+\frac{4}{p-1}}\left(\frac{p-1}{2}\sqrt{d}\; s\right) \\
& \times \mathrm{H2F1}\left[\frac{1}{2}, \frac{1}{2}\left(1-\frac{4}{p-1}\right), \frac{3}{2}, -\sinh^2\left(\frac{p-1}{2}\sqrt{d}\; s\right)\right] \; ds \\
& - \frac{2\beta}{d(p-1)} \int^\xi s \; ds \\
= \;\; & -\frac{4\beta(p-3)(p+3)}{d\sqrt{d}(p-1)^4} \int^\xi I \; ds + \frac{4\beta(p-3)}{d\sqrt{d}(p-1)^3} \int^\xi II \; ds \\
& + \frac{2\beta(p+3)}{d(p-1)^2} \int^\xi III \; ds - \frac{2\beta}{d(p-1)} \int^\xi IV \; ds
\end{aligned} \tag{C.5}$$

Using the asymptotic expression (C.1), the asymptotic behaviour as $\xi \to \pm\infty$ of the integrands is determined. Then these expressions are integrated.

$$
\begin{aligned}
-\frac{4\beta(p-3)(p+3)}{d\sqrt{d}(p-1)^4}\lim_{\xi\to\pm\infty}\int^{\xi} I\ ds &= -\frac{4\beta(p-3)(p+3)}{d\sqrt{d}(p-1)^4}\int_{\xi}\lim_{\xi\to\pm\infty} I\ ds \\
&= -(\pm 1)^{\frac{p+3}{p-1}}\frac{2^{\frac{-2}{p-1}}\beta\sqrt{\pi}(p-3)(p+3)}{d^2(p-1)^4} \\
&\quad\times\frac{\Gamma\left(\frac{2}{p-1}\right)\Gamma\left(\frac{1}{p-1}\right)}{\Gamma\left(\frac{p+1}{p-1}\right)\Gamma\left(\frac{p+1}{2(p-1)}\right)}e^{\sqrt{d}}|\xi| \qquad \text{(C.6)} \\
\frac{4\beta(p-3)}{d\sqrt{d}(p-1)^3}\lim_{\xi\to\pm\infty}\int^{\xi} II\ ds &= \frac{4\beta(p-3)}{d\sqrt{d}(p-1)^3}\int^{\xi}\lim_{\xi\to\pm\infty} II\ ds \\
&= \pm\frac{2^{\frac{p-3}{p-1}}\sqrt{\pi}\beta(p-3)}{d^2(p-1)^3}\frac{\Gamma\left(\frac{1}{p-1}\right)}{\Gamma\left(\frac{p+1}{2(p-1)}\right)}e^{\sqrt{d}|\xi|} \qquad \text{(C.7)} \\
\frac{2\beta(p+3)}{d(p-1)^2}\lim_{\xi\to\pm\infty}\int^{\xi} III\ ds &= \frac{2\beta(p+3)}{d(p-1)^2}\int^{\xi}\lim_{\xi\to\pm\infty} III\ ds \\
&= \frac{\beta(p+3)}{2d(p-1)^2}\frac{\Gamma\left(\frac{2}{p-1}\right)}{\Gamma\left(\frac{p+1}{2(p-1)}\right)}\xi^2 \qquad \text{(C.8)} \\
-\frac{2\beta}{d(p-1)}\lim_{\xi\to\pm\infty}\int^{\xi} IV\ ds &= -\frac{2\beta}{d(p-1)}\int^{\xi}\lim_{\xi\to\pm\infty} IV\ ds \\
&= -\frac{\beta}{d(p-1)}\xi^2 \qquad \text{(C.9)}
\end{aligned}
$$

Now we multiply these results with the asymptotic expression (C.4). Note that then the terms (C.8) and (C.9) vanish. The expressions (C.6) and (C.7) converge to a constant. Therefore, as $\xi\to\pm\infty$, we have

$$
\begin{aligned}
\psi_1\int^{\xi}\psi_2\ g\ ds &= \frac{\beta\sqrt{\pi}(p-3)}{d\sqrt{d}(p-1)^3}\frac{\Gamma\left(\frac{1}{p-1}\right)}{\Gamma\left(\frac{p+1}{2(p-1)}\right)}\left(\frac{d(p+1}{2}\right)^{\frac{1}{p-1}} \\
&\quad\times\left[(\pm 1)^{\frac{p+3}{p-1}}\frac{p+3}{p-1}\frac{\Gamma\left(\frac{2}{p-1}\right)}{\Gamma\left(\frac{p+1}{p-1}\right)}\pm 2\right] \qquad \text{(C.10)}
\end{aligned}
$$

Summarizing, the asymptotics of the term $\psi_2\left(A_2+\int^{\xi}\psi_1\ g\ ds\right)+\psi_1\int^{\xi}\psi_2\ g\ ds$ as $\xi\to\pm\infty$ are given by

$$\lim_{\xi\to\pm\infty}\psi_2\left(A_2+\int_0^{\xi}\psi_1\ g\ ds\right)+\psi_1\int^{\xi}\psi_2\ g\ ds= \tag{C.11}$$

$$e^{\sqrt{d}|\xi|}2^{-\frac{2}{p-1}}\left[\frac{\beta\sqrt{\pi}(p-5)}{2\sqrt{d}(p-1)^2}\frac{\Gamma\left(\frac{2}{p-1}\right)}{\Gamma\left(\frac{p+3}{2(p-1)}\right)}-A_2\left(\frac{d(p+1)}{2}\right)^{-\frac{2}{p-1}}\right]$$

$$\times\left\{(\pm1)^{\frac{4}{p-1}}\frac{3+p}{d(p-1)^2}\frac{\Gamma\left(\frac{2}{p-1}\right)}{\Gamma\left(\frac{p+1}{p-1}\right)}\left(\frac{d(p+1)}{2}\right)^{\frac{1}{p-1}}\mp\frac{2}{d(p-1)}\left(\frac{d(p+1)}{2}\right)^{\frac{1}{p-1}}\right\}$$

$$+\frac{\sqrt{\pi}\beta(p-3)}{d\sqrt{d}(p-1)^3}\left(\frac{d(p+1)}{2}\right)^{\frac{1}{p-1}}\frac{\Gamma\left(\frac{1}{p-1}\right)}{\Gamma\left(\frac{p+1}{2(p-1)}\right)}\left[\frac{3+p}{p-1}\frac{\Gamma\left(\frac{2}{p-1}\right)}{\Gamma\left(\frac{p+1}{p-1}\right)}\left((\pm1)^{\frac{p+3}{p-1}}\mp1\right)+2\left(-(\pm1)^{\frac{4}{p-1}}\pm1\right)\right]$$

D Appendix: asymptotics in the intermediate region

In this chapter the asymptotics of the integrals in the solutions (3.25) and (3.26) is determined. The three integrals are given by

$$I_0(z) = \int_{C_0} t^{\frac{3-p}{p-1}} e^{zt-\frac{1}{12}t^3}\, dt \tag{D.1}$$

$$I_1(z) = \int_{L_1+L_2} t^{\frac{3-p}{p-1}} e^{zt-\frac{1}{12}t^3}\, dt \tag{D.2}$$

$$I_2(z) = \int_{C_2-C_1} t^{\frac{3-p}{p-1}} e^{zt-\frac{1}{12}t^3}\, dt \tag{D.3}$$

where the different paths of integration are shown in figure 12.

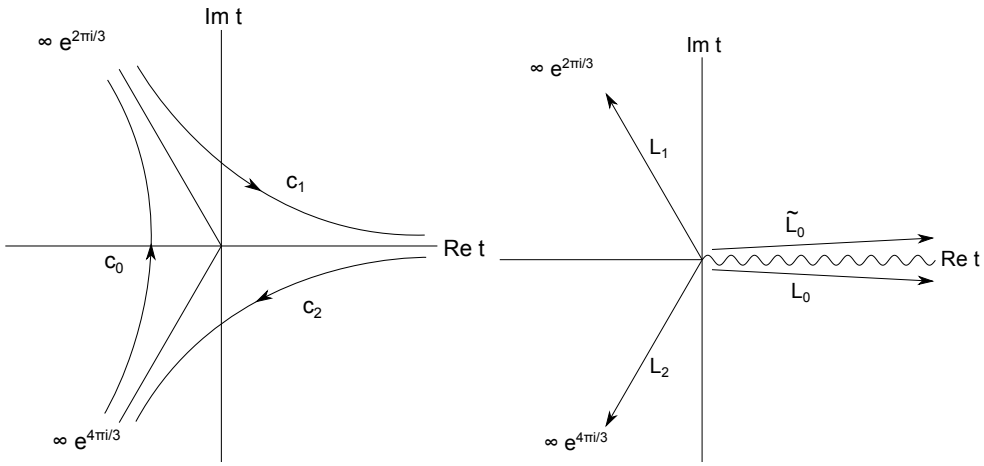

Figure 12: The integration paths C_i and L_i.

First, the asymptotic expressions as $z \to \infty$, with $z > 0$, will be determined. For the first two integrals, (D.1) and (D.3), this will be done using the saddle-point method.

First, we start by explaining the saddle-point method. Suppose we have an integral of the form

$$I(A) = \int_C f(s) e^{A(g(s))} ds, \tag{D.4}$$

with $g(s), f(s)$ complex analytic functions of a complex variable and C some path in the complex plane. We are interested in the behaviour when A is large. Due to the theorem of Cauchy, path integrals of analytic functions are invariant under any deformation when the end points are not affected. The saddle-point method makes use of this fundamental principle. The path C is deformed such that the maximum of $Re(g(s))$ is also a stationary point of $Im(g(s))$. The points that satisfy these conditions are the zeros of the complex derivative $g'(s)$. A properly chosen path starts in an area with a lower value of $Re(g(s))$, reaches the maximum and goes down into another area with a lower value of $Re(g(s))$, this is called a mountain-pass. Near such saddle point, $Re(g(s))$ looks like a saddle, which is where the name of the method comes from.

We denote the saddle-point by s_0 and change the integration variable into

$$s = s_0 + \frac{\eta y}{\sqrt{A}},$$

where η a unimodular complex number, $|\eta| = 1$. This shifts the saddle-point to $y = 0$.

Then, we expand the integrand of (D.4) into powers of $\frac{1}{\sqrt{A}}$

$$I(A) = \frac{\eta f(s_0) e^{Ag(s_0)}}{\sqrt{A}} \int_{\tilde{C}} e^{\frac{y^2\eta^2 g''(s_0)}{2}} \left(1 + \sum_{n=1}^{\infty} \eta^{-n} A^{-\frac{n}{2}} P_n(y)\right) \, dy. \tag{D.5}$$

Here, $\tilde{C}$ is the new integration contour in the y-plane, which always goes through the point $y = 0$. However, the direction of that passing depends on η. For simplicity, let us choose η in such a way that $\tilde{C}$ is tangent to the real axis at $y = 0$. As A grows large, all points on the contour $\tilde{C}$ scale as $\sqrt{A}$, so if it is tangent to the real axis for finite A, the contour $\tilde{C}$ becomes the real axis as $A \to \infty$. Contributions of very large y do not affect the asymptotic behaviour of the integral $I(A)$, hence, for large A,

$$\begin{aligned} I(A) &= \frac{\eta f(s_0) e^{Ag(s_0)}}{\sqrt{A}} \int_{-\infty}^{\infty} e^{\frac{y^2\eta^2 g''(s_0)}{2}} \left(1 + \sum_{n=1}^{\infty} n^{-\eta} A^{-\frac{n}{2}} P_n(y)\right) \, dy \\ &= \sqrt{\frac{2\pi}{A}} e^{Ag(s_0)} \frac{\eta f(s_0)}{\sqrt{-\eta^2 g''(s_0)}} \left(1 + \mathcal{O}\left(\frac{1}{A}\right)\right). \end{aligned} \tag{D.6}$$

The way we choose η assures that the real part of $\eta^2 g''(s_0) < 0$.

Now we apply this method to the integrals (D.1) and (D.3). We start by transforming the variables to obtain integrals of the form of (D.4). Therefore, introduce $\lambda^2 = z$ and $t = \lambda s$

$$I_0(z) = \lambda^{\frac{2}{p-1}} \int_{C_0} s^{\frac{3-p}{p-1}} e^{\lambda^3\left(zs - \frac{1}{12}s^3\right)} \, ds \tag{D.7}$$

$$I_2(z) = \lambda^{\frac{2}{p-1}} \int_{C_2 - C_1} s^{\frac{3-p}{p-1}} e^{\lambda\left(zs - \frac{1}{12}s^3\right)} \, ds. \tag{D.8}$$

For positive z, hence, real λ, we define $g(s) = s - \frac{1}{12}s^3$, which has saddle points at $s = \pm 2$. Since $g(2) = \frac{4}{3} > \frac{-4}{3} = g(-2)$, the positive saddle point seems to be dominant. However, this dominance only works for paths that intersect that point in a mountain-pass like. Since $g(2) = -1$, this means that the contour would have to intersect the saddle point within $\frac{\pi}{4}$ of the horizontal axis. Setting $\eta = 1$, the paths $-C_1$ and C_2 are deformed such that the new paths intersect the point $s = 2$ horizontally. Hence, using the asymptotic expression (D.6) and substituting $z = \lambda^2$ back, the integral (D.8) becomes

$$I_2(z) = 2^{\frac{2}{p-1}} \sqrt{2\pi} z^{\frac{1}{p-1} - \frac{3}{4}} e^{\frac{4}{3}z^{\frac{3}{2}}} \left(1 + \mathcal{O}\left(z^{-\frac{3}{2}}\right)\right). \tag{D.9}$$

The asymptotics of the integral (D.7) is controlled by the other saddle-point, $s_0 = -2$. Since $g''(-2) = 1$, we want the contour to intersect this point in a direction within $\frac{\pi}{4}$ of

the vertical axis. Given the general upward direction of the path C_0, this suggest $\eta = i$ for the deformed contour that intersects $s = -2$. So, for large z, using the asymptotic expression (D.6) and substituting $z = \lambda^2$ back, this yields for integral (D.7)

$$I_0(z) = e^{\frac{(5-p)i\pi)}{2(p-1)}} 2^{[\frac{5-p}{2(p-1)}} z^{\frac{1}{p-1}-\frac{3}{4}} e^{-\frac{4}{3}z^{\frac{3}{2}}} \left(1 + \mathcal{O}\left(z^{-\frac{3}{2}}\right)\right). \tag{D.10}$$

For negative z, we have $g(s) = -s - \frac{1}{12}s^3$, which has saddle-points at $s = \pm 2i$. Both saddle-points have $Re(g(s)_{s=\pm 2i}) = 0$, so we expect them to be co-dominant. Using the general direction of the paths in figure 12, we choose the deformed C_0 such that it intersects the upper saddle-point with $\eta = e^{\frac{3\pi i}{4}}$ and the lower saddle-point with $\eta = \frac{\pi i}{4}$. Hence, using (D.6) and substituting z back, integral (D.7) behaves, for large negative z, as

$$I_0(z) = 2^{\frac{2}{p-1}} z^{\frac{1}{p-1}-\frac{4}{3}} \sqrt{2\pi} \sin\left(\frac{4}{3}|z|^{\frac{3}{2}} + \frac{\pi}{4} - \frac{(3-p)\pi}{2(p-1)}\right), \tag{D.11}$$

to leading order.

The integral (D.8) can be studied in a similar way. The deformed C_2 path should intersect only the lower saddle-point, $s_0 = -2i$, with $\eta = \frac{\pi i}{4}$, while the deformed $-C_1$ path should intersect only the upper saddle-point, $s_0 = 2i$, with $e^{-\frac{\pi i}{4}}$. Therefore, using (D.6) and using that $\lambda^2 = z$, integral (D.8) becomes, for large negative z,

$$I_2(z) = 2^{\frac{2}{p-1}} \sqrt{2\pi} z^{\frac{1}{p-1}-\frac{3}{4}} \cos\left(\frac{4}{3}|z|^{\frac{3}{2}} + \frac{\pi}{4} - \frac{(3-p)\pi}{2(p-1)}\right), \tag{D.12}$$

to leading order.

Finally, the asymptotics of (D.2) will be determined, which will be further research.

Since the matching procedure will be done for $p = 5$, the asymptotic expressions will be shown separately here. From expression [10.4.58] of [2], the expansions of the Airy functions are known for $z \gg 1$. Recall that $z = -\left(\frac{\beta}{4}\right)^{\frac{1}{3}} L^{\frac{\gamma}{3}} \left(\xi - \frac{d}{\beta} L^{-1}\right)$ and $\xi_{tp} = \frac{d}{\beta} L^{-\gamma}$.

For $z > 0$ or equivalently $\xi \ll \xi_{tp}$ the asymptotics are given by

$$\begin{aligned}
A_i^2(z) &\sim \tfrac{1}{4}\pi^{-1} z^{-\frac{1}{2}} e^{-\frac{4}{3}z^{\frac{3}{2}}} \\
A_i^2(\xi) &\sim \tfrac{1}{4}\pi^{-1} 2^{\frac{1}{3}} \beta^{-\frac{1}{6}} L^{-\frac{\gamma}{6}} (\xi_{tp} - \xi)^{-\frac{1}{2}} e^{-\frac{2}{3}\beta^{\frac{1}{2}} L^{\frac{\gamma}{2}} (\xi_{tp}-\xi)^{\frac{3}{2}}} \\
\\
B_i^2(z) &\sim \pi^{-1} z^{-\frac{1}{2}} e^{\frac{4}{3}z^{\frac{3}{2}}} \\
B_i^2(\xi) &\sim \pi^{-1} 2^{\frac{1}{3}} \beta^{-\frac{1}{6}} L^{-\frac{\gamma}{6}} (\xi_{tp} - \xi)^{-\frac{1}{2}} e^{\frac{2}{3}\beta^{\frac{1}{2}} L^{\frac{\gamma}{2}} (\xi_{tp}-\xi)^{\frac{3}{2}}} \\
\\
A_i(z)B_i(z) &\sim \tfrac{1}{2}\pi^{-1} z^{-\frac{1}{2}} \\
A_i(\xi)B_i(\xi) &\sim 2^{-1}\pi^{-1} \left[2^{-\frac{2}{3}} \beta^{\frac{1}{3}} L^{\frac{\gamma}{3}} \left(\xi - \tfrac{d}{\beta} L^{-1}\right)\right]^{-\frac{1}{2}}
\end{aligned}$$

For $z < 0$ or $\xi \gg \xi_{tp}$ the asymptotics are given by

$$
\begin{aligned}
A_i^2(z) &\sim \pi^{-1} z^{-\frac{1}{2}} \left[\sin\left(\tfrac{2}{3} z^{\frac{3}{2}} + \tfrac{\pi}{4}\right) - \cos\left(\tfrac{2}{3} z^{\frac{3}{2}} + \tfrac{\pi}{4}\right) \left(\tfrac{2}{3} z^{\frac{3}{2}}\right)^{-1} \right]^2 \\
&\sim \pi^{-1} z^{-\frac{1}{2}} \sin^2\left(\tfrac{2}{3} z^{\frac{3}{2}} + \tfrac{\pi}{4}\right) + \cdots \\
A_i^2(\xi) &\sim \pi^{-1} \left[\left(\tfrac{\beta}{4}\right)^{\frac{1}{3}} L^{\frac{\gamma}{3}} (\xi_{tp} - \xi) \right]^{-\frac{1}{2}} \\
&\quad \cdot \sin^2\left(\tfrac{2}{3} \left[\left(\tfrac{\beta}{4}\right)^{\frac{1}{3}} L^{\frac{\gamma}{3}} (\xi_{tp} - \xi) \right]^{\frac{3}{2}} + \tfrac{\pi}{4} \right) + \cdots
\end{aligned}
$$

$$
\begin{aligned}
B_i^2(z) &\sim \pi^{-1} z^{-\frac{1}{2}} \left[\cos\left(\tfrac{2}{3} z^{\frac{3}{2}} + \tfrac{\pi}{4}\right) + \sin\left(\tfrac{2}{3} z^{\frac{3}{2}} + \tfrac{\pi}{4}\right) \left(\tfrac{2}{3} z^{\frac{3}{2}}\right)^{-1} \right]^2 \\
&\sim \pi^{-1} z^{-\frac{1}{2}} \cos^2\left(\tfrac{2}{3} z^{\frac{3}{2}} + \tfrac{\pi}{4}\right) + \cdots \\
B_i^2(\xi) &\sim \pi^{-1} \left[\left(\tfrac{\beta}{4}\right)^{\frac{1}{3}} L^{\frac{\gamma}{3}} (\xi_{tp} - \xi) \right]^{-\frac{1}{2}} \\
&\quad \cdot \cos^2\left(\tfrac{2}{3} \left[\left(\tfrac{\beta}{4}\right)^{\frac{1}{3}} L^{\frac{\gamma}{3}} (\xi_{tp} - \xi) \right]^{\frac{3}{2}} + \tfrac{\pi}{4} \right) + \cdots
\end{aligned}
$$

$$
\begin{aligned}
A_i(z) B_i(z) &\sim \pi^{-1} z^{-\frac{1}{2}} \left[\sin\left(\tfrac{2}{3} z^{\frac{3}{2}} + \tfrac{\pi}{4}\right) - \cos\left(\tfrac{2}{3} z^{\frac{3}{2}} + \tfrac{\pi}{4}\right) \left(\tfrac{2}{3} z^{\frac{3}{2}}\right)^{-1} \right] \\
&\quad \left[\cos\left(\tfrac{2}{3} z^{\frac{3}{2}} + \tfrac{\pi}{4}\right) + \sin\left(\tfrac{2}{3} z^{\frac{3}{2}} + \tfrac{\pi}{4}\right) \left(\tfrac{2}{3} z^{\frac{3}{2}}\right)^{-1} \right] \\
A_i(\xi) B_i(\xi) &\sim \pi^{-1} \left[\left(\tfrac{\beta}{4}\right)^{\frac{1}{3}} L^{\frac{\gamma}{3}} (\xi_{tp} - \xi) \right]^{-\frac{1}{2}} \sin\left(\tfrac{2}{3} \left[\left(\tfrac{\beta}{4}\right)^{\frac{1}{3}} L^{\frac{\gamma}{3}} (\xi_{tp} - \xi) \right]^{\frac{3}{2}} + \tfrac{\pi}{4} \right) \\
&\quad \cos\left(\tfrac{2}{3} \left[\left(\tfrac{\beta}{4}\right)^{\frac{1}{3}} L^{\frac{\gamma}{3}} (\xi_{tp} - \xi) \right]^{\frac{3}{2}} + \tfrac{\pi}{4} \right) + \cdots
\end{aligned}
$$

with $\tilde{\xi} = \left(\frac{\beta}{4}\right)^{\frac{1}{3}} L^{\frac{\gamma}{3}} (\xi_{tp} - \xi) + \frac{\pi}{4}$.

References

[1] M.J. Ablowitz, M. Kruskal, and H. Segur. A note on miura's transformation. *J. Math. Phys.*, 20, 1979.

[2] M. Abramowitz and I. A. Stegun. *Handbook of Mathematical Functions with Formulas, Graphs, and Mathematical Tables.* Dover, New York, ninth dover printing, tenth gpo printing edition, 1964.

[3] J. L. Bona, P. E. Souganidis, and W. A. Strauss. Stability and instability of solitary waves of korteweg-de vries type. *Proceedings of the Royal Society of London. A. Mathematical and Physical Sciences*, 411(1841):395–412, 1987.

[4] P. Deift and X. Zhou. A steepest descent method for oscillatory riemann-hilbert problems. asymptotics for the mkdv equation. *Annals of Math.*, pages 295 – 368, 1993.

[5] D. B. Dix and W. R. McKinney. Numerical computations of self-similar blow-up solutions of the generalized korteweg-de vries equation.

[6] D.J. Korteweg and G. de Vries. On the change of form of long waves advancing in a rectangular canal, and on a new type of long stationary waves. *Philosophical Magazine*, 5(39):422–443, 1895.

[7] P. D. Lax. Integrals of nonlinear equations of evolution and solitary waves. *Communications on pure and applied mathematics*, 21:pp. 467–490, 1968.

[8] Y. Martel and F. Merle. Blow up in finite time and dynamics of blow up solutions for the l^2-critical generalized kdv equation. *J.Amer. Math. Soc.*, 15:617–664, 2002.

[9] Y. Martel and F. Merle. Stability of blow-up profile and lower bounds for blow-up rate for the critical generalized kdv equation. *The Annals of Mathematics*, 155(1):pp. 235–280, 2002.

[10] F. Merle. Existence of blow-up solutions in the energy space for the critical generalized kdv equation. *J.Amer. Math. Soc.*, 14:555–578, 2001.

[11] R.M. Miura. The korteweg-de vries equation: A survey of results. *SIAM Review*, 18(3):pp. 412–459, 1976.

[12] R.L. Pego and M.I. Weinstein. Eigenvalues and instabilities of solitary waves. *Phil. Trans. R. Soc. Lond.*, A 340:47 – 94, 1992.

[13] W.H. Reid. Integral representations for products of airy functions. *Zeitschrift fr Angewandte Mathematik und Physik*, 48 (4):646–655.

[14] V. Rottschäfer. Asymptotic analysis of a new type of multi-bump, self-similar, blowup solutions of the ginzburg landau equation. *Technical Report 2011-15 MI Leiden*, 2011, submitted.

[15] P.C. Schuur. *Asymptotic Analysis of Soliton Problems*. Springer Verlag, Berlin, 1986.

[16] T. Tao. Why are solitons stable?, 2009.

[17] O. Vallée. *On the linear third-order differential equation*, volume 518 of *Lecture Notes in Physics*. Springer Berlin / Heidelberg, 1999. 10.1007/BFb0105940.